

chapter 1

multipath interference

W. C. Jakes

SYNOPSIS OF CHAPTER

Nature is seldom kind. One of the most appealing uses for radio-telephone systems—communication with people on the move—must overcome radio transmission problems so difficult they challenge the imagination. A microwave radio signal transmitted between a fixed base station and a moving vehicle in a typical urban environment exhibits extreme variations in both amplitude and apparent frequency. Fades of 40 dB or more below the mean level are common, with successive minima occurring about every half wavelength (every few inches) of the carrier transmission frequency. A vehicle driving through this fading pattern at speeds up to 60 mi/hr can experience random signal fluctuations occurring at rates of 100–1000 Hz, thus distorting speech when transmitted by conventional methods. These effects are due to the random distribution of the field in space, and arise directly from the motion of the vehicle. If the vehicle is stationary the fluctuation rates are orders of magnitude less severe.

These observations seem to defy any attempt at a systematic interpretation or quantitative analysis. However, starting from a model based on multipath wave interference, arising from multiple scattering of the waves by the buildings and other structures in the vicinity of the mobile unit, we shall see that a great many of the observable properties of the transmission can be successfully predicted by using the powerful techniques of statistical communication theory. The fundamental relationships are established in Section 1.1, where the fields are expressed as a linear superposition of plane waves of random phase. This leads directly to expressions giving the probability that the signal envelope can be expected to be found within a narrow range around a given level (probability density), and the percent of time it lies below a given level (cumulative distribution).

Besides a random phase, each component plane wave has associated with it a Doppler shift depending on the mobile speed, the carrier frequency, and the angle its propagation vector makes with the mobile

velocity vector. This implies that the apparent power spectrum of each of the three received field components is broadened to occupy a narrow band about the carrier frequency. General expressions for the shapes of these power spectra are derived in Section 1.2 and show their dependence on the assumed density of the arrival angles and the mobile antenna directivity pattern. As a by-product of these derivations it is also shown that, with relatively loose restrictions on the distribution of arrival angles, the three field components are statistically uncorrelated if they are observed simultaneously.

The radio frequency characteristics of signals are usually somewhat difficult to observe; the signal envelope is more directly accessible. A number of properties of the fading signal envelopes associated with the mobile transmission path are derived in Section 1.3. Some general correlations and statistical moments of the in-phase and quadrature signal components are presented, preparatory to deriving the power spectrum of the envelope from the Fourier transform of its autocorrelation. The inclusion of a small steady signal from the base station is shown to explain some observed fine structure in the power spectra. The rate at which the envelope crosses a specified signal level is frequently of interest; expressions are presented for this property, along with expressions for the average length of time the envelope spends below a specified level. Finally, the auto- and cross-covariance functions for the envelopes of the three electromagnetic field components are derived, and it is shown how they may be interpreted in terms of spatial instead of time coordinates.

The instantaneous frequency of the signal received at the mobile undergoes rapid, random variations due to the variations of the in-phase and quadrature signal components. This random frequency modulation is explored in Section 1.4, where its probability density and cumulative distribution are derived first. The larger frequency deviations are shown to coincide with the deeper fades and are many times larger than the Doppler shift of any of the constituent plane waves. The power spectrum of the random frequency modulation is also derived; beyond a frequency equal to twice the maximum possible Doppler shift it drops as $1/f$.

If two carriers are transmitted from the base station at slightly different frequencies, then their statistical properties, as observed at the mobile antenna, are independent if the frequency separation is large enough. The frequency separation for which the signals are still strongly correlated is called the coherence bandwidth, and is studied in Section 1.5. The basic mechanism responsible for this property is shown to be the difference in propagation time delays associated with the various scattered waves making up the total signal. The relationship between the coherence bandwidth

and the standard deviation of the time delay distribution is developed and compared with measurements for several models of the delay distribution. Expressions are derived for the correlation of the carrier amplitudes and phases as a function of the frequency separation.

The auto-covariance of any field component envelope measured at two separate points on the mobile is shown in Section 1.3 to decrease rapidly as the spatial separation increases. When the mobile transmits to the base station, however, the analogous auto-covariance measured at the base decreases much more slowly with spatial separation. The reasons for this effect are studied in Section 1.6. They are shown to be related to the geometrical asymmetry in the mobile-base transmission path, which arises because the base antenna is usually located well above any nearby scattering objects. Theoretical expressions for the auto-covariance are derived and compared with the relatively few measurements available.

The final acceptability of mobile radio systems is usually established by tests in the field. Preliminary comparisons between alternative system designs would be considerably expedited if such tests could be carried out in the laboratory, using signals that provide the same characteristics of the fading signals observed in the field. A simulation scheme is described in Section 1.7 that duplicates the envelope fading statistics, correlation function, power spectrum, and random frequency modulation of the mobile radio signal. The method is patterned after the basic multipath interference model described in Section 1.1. The validity of the technique is established by appropriate statistical measurements.

1.1 SPATIAL DISTRIBUTION OF THE FIELD

1.1.1 Envelope Measurements and Mathematical Model

One readily accessible property of the signal transmitted over a mobile radio propagation path is the amplitude variation of its envelope as the position of the mobile terminal is moved. This information is generally presented in the form of time recordings of the signal level; with uniform vehicle motion there is, of course, a 1 : 1 correspondence between distance measured on the recording and distance traveled in the street. A typical recording¹ is shown in Figure 1.1-1 for a run made at 836 MHz in a suburban environment. The occasional deep fades and quasiperiodic occurrence of minima are clearly evident in the expanded section of the record.

Recordings such as these made by many workers in the field over the frequency range from 50 to 11,200 MHz have shown that the envelope of the mobile radio signal is Rayleigh distributed²⁻⁵ when measured over

distances of a few tens of wavelengths where the mean signal is sensibly constant. This suggests the assumption,⁶ reasonable on physical grounds, that at any point the received field is made up of a number of horizontally traveling plane waves with random amplitudes and angles of arrival for different locations. The phases of the waves are uniformly distributed from 0 to 2π . The amplitudes and phases are assumed to be statistically independent. Other models have also been proposed,⁷ but they lead to comparable statistical properties of the field for large numbers of constituent waves.

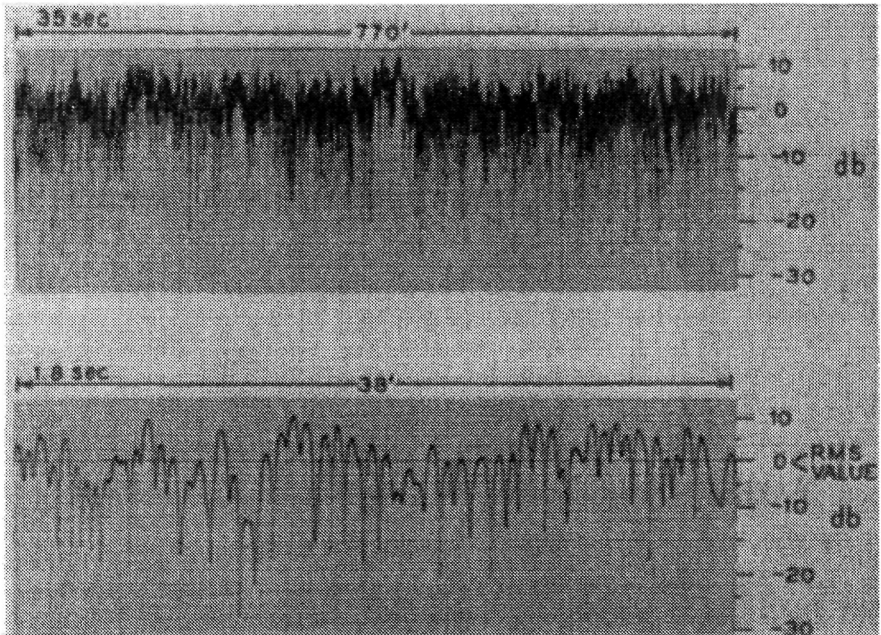


Figure 1.1-1 Typical received signal variations at 836 MHz measured at a mobile speed of 15 miles/hr. Records taken on the same street with different recording speeds.

A diagram of this simple model is shown in Figure 1.1-2 with plane waves from stationary scatterers incident on a mobile traveling in the x -direction with velocity v . The x - y plane is assumed to be horizontal. The vehicle motion introduces a Doppler shift in every wave:

$$\omega_n = \beta v \cos \alpha_n, \quad (1.1-1)$$

where $\beta = 2\pi/\lambda$, λ being the wavelength of the transmitted carrier frequency.

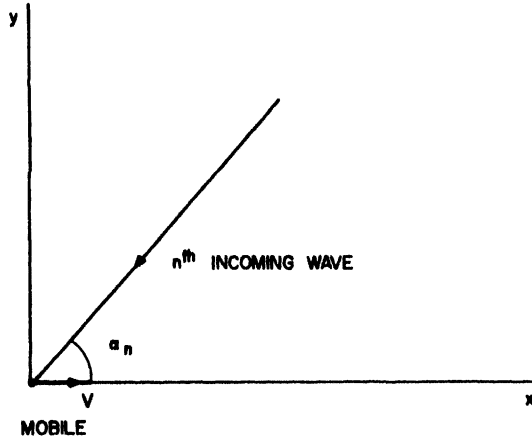


Figure 1.1-2 A typical component wave incident on the mobile receiver.

If the transmitted signal is vertically polarized, the field components seen at the mobile can thus be written

$$E_z = E_0 \sum_{n=1}^N C_n \cos(\omega_c t + \theta_n), \tag{1.1-2}$$

$$H_x = -\frac{E_0}{\eta} \sum_{n=1}^N C_n \sin \alpha_n \cos(\omega_c t + \theta_n), \tag{1.1-3}$$

$$H_y = \frac{E_0}{\eta} \sum_{n=1}^N C_n \cos \alpha_n \cos(\omega_c t + \theta_n), \tag{1.1-4}$$

where

$$\theta_n = \omega_c t + \phi_n, \tag{1.1-5}$$

and ω_c is the carrier frequency of the transmitted signal, η is the free-space wave impedance, $E_0 C_n$ is the (real) amplitude of the n th wave in the E_z field. The ϕ_n are random phase angles uniformly distributed from 0 to 2π . Furthermore, the C_n are normalized so that the ensemble average $\langle \sum_{n=1}^N C_n^2 \rangle = 1$.

We note from Eq. (1.1-1) that the Doppler shift is bounded by the values $\pm \beta v$ which, in general, will be very much less than the carrier frequency. For example, for $f_c = \omega_c/2\pi = 1000$ MHz, $v = 60$ mi/hr:

$$\frac{1}{2\pi}\beta v = \frac{v}{\lambda} \doteq 90 \text{ Hz.} \quad (1.1-6)$$

The three field components may thus be described as narrow-band random processes. Furthermore, as a consequence of the central limit theorem, for large values of N they are approximately Gaussian random processes, and the considerable body of literature devoted to such processes may be utilized. It must be kept in mind that this is still an approximation; for example, Eq. (1.1-2) implies that the mean signal power is constant with time, whereas it actually undergoes slow variations as the mobile moves distances of hundreds of feet. Nevertheless, the Gaussian model is successful in predicting the measured statistics of the signal to good accuracy in most cases over the ranges of interest for the variables involved; thus its use is justified.

Following Rice⁸ we can express E_z as

$$E_z = T_c(t) \cos \omega_c t - T_s(t) \sin \omega_c t, \quad (1.1-7)$$

where

$$T_c(t) = E_0 \sum_{n=1}^N C_n \cos(\omega_n t + \phi_n), \quad (1.1-8)$$

$$T_s(t) = E_0 \sum_{n=1}^N C_n \sin(\omega_n t + \phi_n), \quad (1.1-9)$$

are Gaussian random processes, corresponding to the in-phase and quadrature components of E_z , respectively. We denote by T_c and T_s the random variables corresponding to $T_c(t)$ and $T_s(t)$ for fixed t . They have zero mean and equal variance:

$$\langle T_c^2 \rangle = \langle T_s^2 \rangle = \frac{E_0^2}{2} = \langle |E_z|^2 \rangle. \quad (1.1-10)$$

The brackets indicate an ensemble average over the α_n , ϕ_n , and C_n . T_c and T_s are also uncorrelated (and therefore independent):

$$\langle T_c T_s \rangle = 0. \quad (1.1-11)$$

1.1.2 Probability Distributions

Since T_c and T_s are Gaussian, they have probability densities of the form

$$p(x) = \frac{1}{\sqrt{2\pi b}} e^{-x^2/2b} \tag{1.1-12}$$

where $b = E_0^2/2$ is the mean power, and $x = T_c$ or T_s .

The envelope of E_z is given by

$$r = (T_c^2 + T_s^2)^{1/2}, \tag{1.1-13}$$

and Rice⁸ has shown that the probability density of r is

$$p(r) = \begin{cases} \frac{r}{b} e^{-r^2/2b}, & r \geq 0 \\ 0, & r < 0 \end{cases} \tag{1.1-14}$$

which is the Rayleigh density formula. The Gaussian and Rayleigh densities are shown in Figure 1.1-3 for illustration.

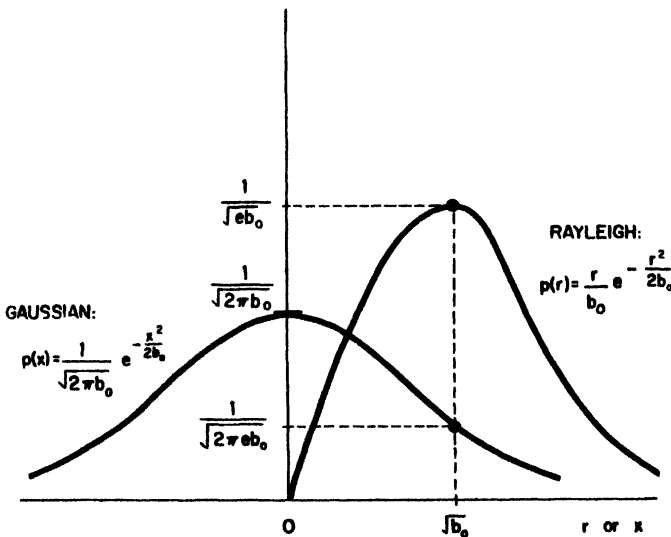


Figure 1.1-3 Gaussian and Rayleigh probability density functions.

The cumulative distribution functions of T_c (or T_s) are also of interest:

$$P[x < X] = \int_{-\infty}^X p(x) dx = \frac{1}{2} \left[1 + \operatorname{erf} \left(\frac{X}{\sqrt{2b}} \right) \right], \quad (1.1-15)$$

where the error function is defined by

$$\operatorname{erf}(y) = \frac{2}{\sqrt{\pi}} \int_0^y e^{-t^2} dt. \quad (1.1-16)$$

Similarly for the envelope,

$$P[r < R] = \int_{-\infty}^R p(r) dr = 1 - e^{-R^2/2b}. \quad (1.1-17)$$

These distribution functions are illustrated in Figure 1.1-4.

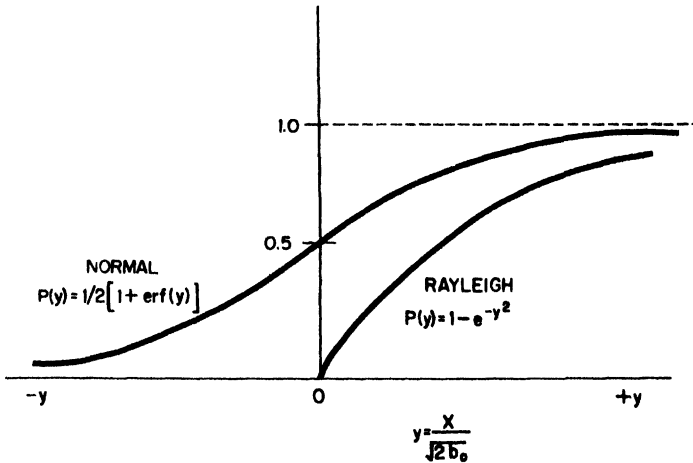


Figure 1.1-4 Normal and Rayleigh cumulative distributions.

Thus the simple model has predicted the widely observed Rayleigh nature of the fading. Some of the measurements are shown in Figure 1.1-5 for tests made at 836 and 11,200 MHz in a suburban area.¹ The coordinates in Figure 1.1-5 are scaled so that the Rayleigh cumulative distribution appears as a straight line.

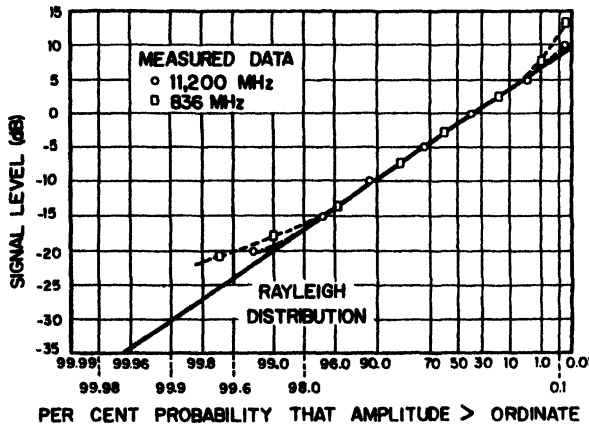


Figure 1.1-5 Cumulative probability distributions for 836 and 11,200 MHz.

The random processes T_c and T_s defined by Eqs. (1.1-8) and (1.1-9) will form the basis for much of the statistical analysis to follow in succeeding sections of this chapter. Arguments were advanced earlier to justify the assumption that they are Gaussian random processes. In addition, for times that are short compared to the slow variations it will be assumed that they are wide-sense stationary; since they are assumed to be Gaussian this implies that they are stationary in the strict sense.⁹ Such processes (e.g., the wide-sense stationary uncorrelated scattering channel of Bello^{10,11}) have been extensively studied, and expressions have been obtained for many statistical properties that will be freely applied in this work. The final justification of these assumptions, of course, is the accuracy with which the analytical results agree with measurements, but in most cases the agreement is good enough to lend credence to the model.

1.2 POWER SPECTRA OF THE FADING SIGNAL

From the viewpoint of an observer on the mobile unit, the signal received from a CW transmission as the mobile moves with constant velocity may be represented as a carrier whose phase and amplitude are randomly varying, with an effective bandwidth corresponding to twice the maximum Doppler shift of βv . Many of the statistical properties of this random process can be determined from its moments, which, in turn, are most easily obtained from the power spectrum.

1.2.1 RF Spectra of the Field Components

We assume that the field may be represented by the sum of N waves, as in Eq. (1.1-2). As $N \rightarrow \infty$ we would expect to find that the incident power included in an angle between α and $\alpha + d\alpha$ would approach a continuous, instead of discrete, distribution. Let us denote by $p(\alpha)d\alpha$ the fraction of the total incoming power within $d\alpha$ of the angle α , and also assume that the receiving antenna is directive in the horizontal plane with power gain pattern $G(\alpha)$. The differential variation of received power with angle is then* $bG(\alpha)p(\alpha)d\alpha$; we equate this to the differential variation of received power with frequency by noting the relationship between frequency and angle of Eq. (1.1-1):

$$f(\alpha) = f_m \cos \alpha + f_c, \quad (1.2-1)$$

where $f_m = \beta v / 2\pi = v / \lambda$, the maximum Doppler shift. Since $f(\alpha) = f(-\alpha)$, the differential variation of power with frequency may be expressed as

$$S(f)|df| = b[p(\alpha)G(\alpha) + p(-\alpha)G(-\alpha)]|d\alpha|. \quad (1.2-2)$$

But

$$|df| = f_m |-\sin \alpha d\alpha| = \sqrt{f_m^2 - (f - f_c)^2} |d\alpha|;$$

thus

$$S(f) = \frac{b}{\sqrt{f_m^2 - (f - f_c)^2}} [p(\alpha)G(\alpha) + p(-\alpha)G(-\alpha)], \quad (1.2-3)$$

where

$$\alpha = \cos^{-1} \left(\frac{f - f_c}{f_m} \right) \quad \text{and} \quad S(f) = 0 \quad \text{if} \quad |f - f_c| > f_m. \quad (1.2-4)$$

Equation (1.2-3) gives the power spectrum of the output of a receiving antenna. In general this power spectrum depends on the antenna gain pattern and differs from the power spectrum of the field components. However, within the assumptions of the present model, there are antennas that respond to the field components directly. For example, we will assume the transmitted signal is vertically polarized. The electric field will then be in the z -direction and may be sensed by a vertical whip antenna on the mobile, with $G(\alpha) = 1.5$. Substituting in Eq. (1.2-3), the power spectrum of

* b is the average power that would be received by an isotropic antenna, that is, $G(\alpha) = 1$.

the electric field is

$$S_{E_z}(f) = \frac{1.5b}{\sqrt{f_m^2 - (f - f_c)^2}} [p(\alpha) + p(-\alpha)]. \quad (1.2-5)$$

Small loops may likewise be used to sense the magnetic field, a loop along the x -axis for H_y , and one along the y -axis for H_x . The assumed antenna patterns are then

$$H_x: \quad G(\alpha) = \frac{3}{2} \sin^2 \alpha, \quad (1.2-6)$$

$$H_y: \quad G(\alpha) = \frac{3}{2} \cos^2 \alpha. \quad (1.2-7)$$

Substituting these in Eq. (1.2-3),

$$S_{H_x}(f) = \frac{1.5b}{f_m^2} \sqrt{f_m^2 - (f - f_c)^2} [p(\alpha) + p(-\alpha)], \quad (1.2-8)$$

$$S_{H_y}(f) = \frac{1.5b(f - f_c)^2}{f_m^2 \sqrt{f_m^2 - (f - f_c)^2}} [p(\alpha) + p(-\alpha)]. \quad (1.2-9)$$

The simplest assumption for the distribution of power with arrival angle α is a uniform distribution:

$$p(\alpha) = \frac{1}{2\pi}, \quad -\pi < \alpha < \pi. \quad (1.2-10)$$

The three power spectra become

$$S_{E_z}(f) = \frac{3b}{\omega_m} \left[1 - \left(\frac{f - f_c}{f_m} \right)^2 \right]^{-1/2} \quad (1.2-11)$$

$$S_{H_x}(f) = \frac{3b}{\omega_m} \left[1 - \left(\frac{f - f_c}{f_m} \right)^2 \right]^{1/2} \quad (1.2-12)$$

$$S_{H_y}(f) = \frac{3b}{\omega_m} \left(\frac{f - f_c}{f_m} \right)^2 \left[1 - \left(\frac{f - f_c}{f_m} \right)^2 \right]^{-1/2} \quad (1.2-13)$$

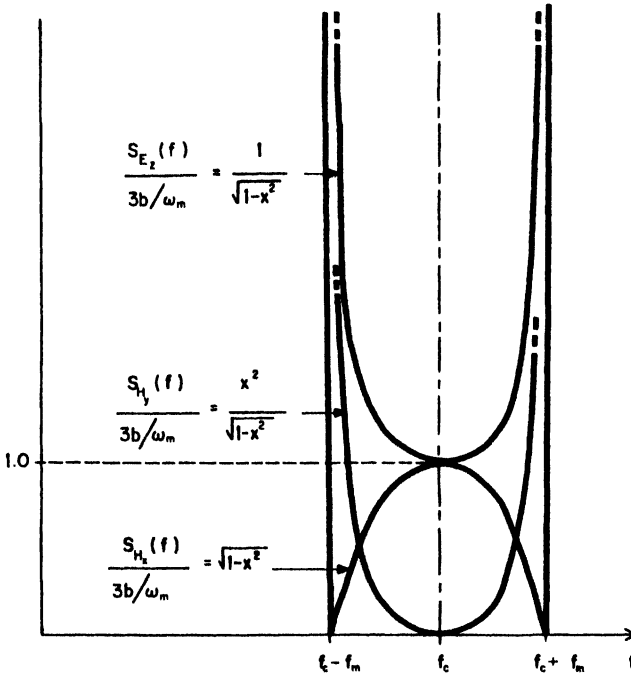


Figure 1.2-1 Power spectra of the three field components for uniformly distributed arrival angles. [$x = (f - f_c)/f_m$]

These spectra are shown in Figure 1.2-1.

Measurement of the RF spectrum is generally very difficult in practice, because of its very small fractional bandwidth of $2v/c$, where c is the velocity of light. Some measurements¹² were made at 910 MHz using oscillators with high frequency stability and yielded the frequency spectrogram of the electric field shown in Figure 1.2-2. Spectral density is shown as dark intensity on the figure, frequency is plotted on the ordinate, and time on the abscissa. The mobile was first stationary, as shown by the narrow line to the left. As the mobile speed increased the trace broadened, and the spectrogram width corresponds very closely to the predicted value of $2v/\lambda$.

1.2.2 Correlations and Cross Spectra of the Field Components

Additional spectra that occasionally are of interest correspond to the cross correlations between the three electromagnetic field components, E_x ,

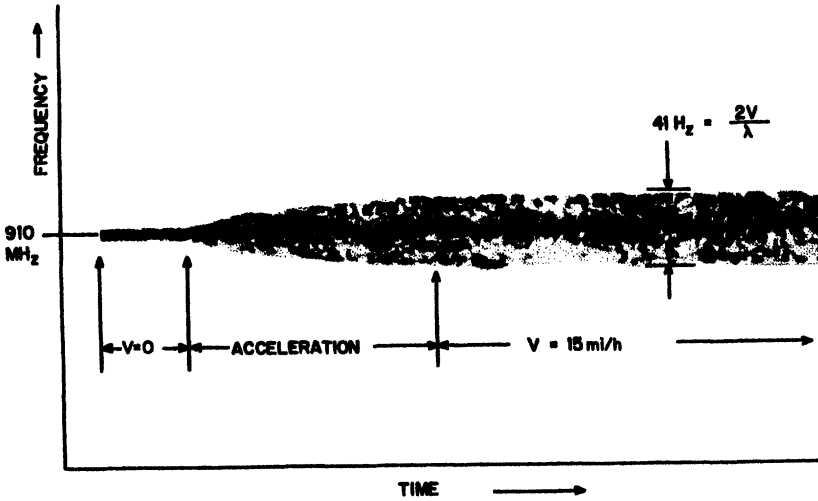


Figure 1.2-2 Frequency spectrogram of RF signal at 910 MHz.

H_x , and H_y . Consider E_z and H_x :

$$\begin{aligned}
 R_{E_z H_x}(\tau) &= \langle E_z(t) H_x(t + \tau) \rangle \\
 &= -\frac{E_0^2}{\eta} \sum_{n,m} C_n C_m \sin \alpha_m \langle \cos[(\omega_c + \omega_n)t + \phi_n] \cos[(\omega_c + \omega_m)(t + \tau) + \phi_m] \rangle.
 \end{aligned}
 \tag{1.2-14}$$

The product of the cosines can be expanded into cosines of the sums and differences of their angles, which includes terms of the form $\phi_m \pm \phi_n$. The ensemble average over these angles is zero except for the terms $\phi_m - \phi_n$ with $m = n$, in which case

$$R_{E_z H_x}(\tau) = -\frac{b}{\eta} \sum_{n=1}^N C_n^2 \sin \alpha_n \cos(\omega_c + \omega_n)\tau.
 \tag{1.2-15}$$

Since $C_n^2 = p(\alpha_n) d\alpha$, in the limit as $N \rightarrow \infty$ we can write

$$R_{E_z H_x}(\tau) = -\frac{b}{\eta} \int_{-\pi}^{\pi} p(\alpha) \sin \alpha \cos(\omega_c \tau + \omega_m \tau \cos \alpha) d\alpha.
 \tag{1.2-16}$$

The integrand is an odd function of α if $p(-\alpha) = p(\alpha)$; thus $R_{E_z H_x}(\tau) = 0$ for any τ if $p(\alpha)$ is even. It can easily be shown also that $R_{H_x H_x}(\tau) = 0$ for any τ if $p(\alpha)$ is even; thus H_x is uncorrelated with both E_z and H_y in this case, and the corresponding cross spectra are also zero. Comparing the

expressions for E_z and H_y , we see that H_y can be regarded as the output from a filter with frequency transfer function

$$H(\omega) = \frac{\cos \alpha}{\eta} = \frac{\omega - \omega_c}{\eta \omega_m}, \quad (1.2-17)$$

whose input is E_z . The cross spectrum in this case is simply given by⁹

$$S_{E_z H_y}(f) = S_{E_z}(f) H^*(f) = \frac{f - f_c}{\eta f_m} S_{E_z}(f). \quad (1.2-18)$$

If $p(\alpha) = 1/2\pi$, then

$$S_{E_z H_y}(f) = \frac{3b}{\eta \omega_m} \left(\frac{f - f_c}{f_m} \right) \left[1 - \left(\frac{f - f_c}{f_m} \right)^2 \right]^{-1/2} \quad (1.2-19)$$

Note that this spectrum is an odd function about the center frequency f_c . The cross correlation of E_z and H_y is

$$\begin{aligned} R_{E_z H_y}(\tau) &= \langle E_z(t) H_y(t + \tau) \rangle \\ &= -\frac{b}{\eta} \int_{-\pi}^{\pi} p(\alpha) \cos \alpha \cos(\omega_c \tau + \omega_m \tau \cos \alpha) d\alpha. \end{aligned} \quad (1.2-20)$$

For $p(\alpha) = 1/2\pi$,

$$R_{E_z H_y}(\tau) = \frac{b}{\eta} \sin \omega_c \tau J_1(\beta v \tau). \quad (1.2-21)$$

Thus we have the important result that all three field components are uncorrelated at $\tau = 0$.

1.3 POWER SPECTRUM AND OTHER PROPERTIES OF THE SIGNAL ENVELOPE

1.3.1 In-Phase and Quadrature Moments

From the expressions for the power spectral densities given in the preceding section we can derive a number of interesting properties of the envelopes corresponding to the three field components, again with the assumption that the incoming power is uniformly distributed in angle. First we need certain correlations and moments of the in-phase and quadrature components of the signal, T_c and T_s . The subscripts 1 and 2 refer to the

times t and $t + \tau$, respectively. Following Rice,⁸

$$\begin{aligned}
 \langle T_{c_1} T_{c_2} \rangle &= \langle T_{s_1} T_{s_2} \rangle = g(\tau), \\
 \langle T_{c_1} T_{s_2} \rangle &= -\langle T_{s_1} T_{c_2} \rangle = h(\tau), \\
 \langle T_{c_1} T_{c_2}' \rangle &= \langle T_{s_1} T_{s_2}' \rangle = -\langle T_{c_1}' T_{c_2} \rangle = -\langle T_{s_1}' T_{s_2} \rangle = g'(\tau), \\
 \langle T_{c_1} T_{s_2}' \rangle &= \langle T_{s_1}' T_{c_2} \rangle = -\langle T_{c_1}' T_{s_2} \rangle = -\langle T_{s_1} T_{c_2}' \rangle = h'(\tau), \\
 \langle T_{c_1}' T_{c_2}' \rangle &= \langle T_{s_1}' T_{s_2}' \rangle = -g''(\tau), \\
 \langle T_{c_1}' T_{s_2}' \rangle &= -\langle T_{s_1}' T_{c_2}' \rangle = -h''(\tau),
 \end{aligned} \tag{1.3-1}$$

where

$$g(\tau) = \int_{f_c - f_m}^{f_c + f_m} S_i(f) \cos 2\pi(f - f_c)\tau df, \tag{1.3-2}$$

$$h(\tau) = \int_{f_c - f_m}^{f_c + f_m} S_i(f) \sin 2\pi(f - f_c)\tau df, \tag{1.3-3}$$

and $S_i(f)$ is the input spectrum defined for $f_c - f_m < f < f_c + f_m$. (Primes denote differentiation with respect to time.)

From the above correlations evaluated at $\tau = 0$ the moments can also be obtained:

$$b_n = (2\pi)^n \int_{f_c - f_m}^{f_c + f_m} S_i(f) (f - f_c)^n df. \tag{1.3-4}$$

Thus

$$\begin{aligned}
 \langle T_c^2 \rangle &= \langle T_s^2 \rangle = g(0) = b_0, \\
 \langle T_c T_s \rangle &= h(0) = 0, \\
 \langle T_c T_c' \rangle &= \langle T_s T_s' \rangle = g'(0) = 0, \\
 \langle T_c T_s' \rangle &= -\langle T_c' T_s \rangle = h'(0) = b_1, \\
 \langle T_c'^2 \rangle &= \langle T_s'^2 \rangle = -g''(0) = b_2, \\
 \langle T_c' T_s' \rangle &= -h''(0) = 0.
 \end{aligned} \tag{1.3-5}$$

Substituting the expressions for the three spectra given in Eqs. (1.2-11) to (1.2-13) into Eqs. (1.3-2) and (1.3-3):

$$h(\tau) = 0 \quad \text{for all three field components.}$$

(This is a consequence of the symmetry of the spectra about f_c .) All b_n likewise equal zero for n odd.

Electric field:

$$b_n = b_0 \omega_m^n \frac{1 \cdot 3 \cdot 5 \cdots (n-1)}{2 \cdot 4 \cdot 6 \cdots n}, \quad b_0 = 1.5b = \frac{3E_0^2}{4} \quad (1.3-6)$$

$$g(\tau) = b_0 J_0(\omega_m \tau). \quad (1.3-7)$$

Magnetic field, x -component:

$$b_n = b_{0H} \omega_m^n \frac{2}{n+2} \frac{1 \cdot 3 \cdot 5 \cdots (n-1)}{2 \cdot 4 \cdot 6 \cdots n}, \quad b_{0H} = \frac{3E_0^2}{8} \quad (1.3-8)$$

$$g(\tau) = b_{0H} [J_0(\omega_m \tau) + J_2(\omega_m \tau)]. \quad (1.3-9)$$

Magnetic field, y -component:

$$b_n = 2b_{0H} \omega_m^n \frac{1 \cdot 3 \cdot 5 \cdots (n+1)}{2 \cdot 4 \cdot 6 \cdots (n+2)}, \quad (1.3-10)$$

$$g(\tau) = b_{0H} [J_0(\omega_m \tau) - J_2(\omega_m \tau)]. \quad (1.3-11)$$

Comparison of b_0 and b_{0H} indicates that the average output power of the loop antenna is 3 dB weaker than that from the vertical dipole.*

1.3.2 General Expression for Envelope Autocorrelation and Spectrum

The autocorrelation function of the envelope, r , of a narrow-band Gaussian process can be expressed in terms of a hypergeometric function (Ref. 13, p. 170):

$$R_r(\tau) = \frac{\pi}{2} b_0 F\left[-\frac{1}{2}, -\frac{1}{2}; 1; \rho^2(\tau)\right], \quad (1.3-12)$$

where

$$\rho^2(\tau) = \frac{1}{b_0^2} [g^2(\tau) + h^2(\tau)] \quad (1.3-13)$$

*Since the vertical dipole will be used often as an example, we do not include the subscript identification, E (i.e., b_{0E} as in b_{0H}) in order to simplify notation.

and $g(\tau)$, $h(\tau)$ are the correlations defined above. At $\tau=0$, $\rho^2(0)=1$; thus

$$R_r(0) = \langle r^2 \rangle = \frac{\pi}{2} b_0 F\left(-\frac{1}{2}, -\frac{1}{2}; 1; 1\right) = 2b_0. \quad (1.3-14)$$

(Note that $\langle r^2 \rangle = \int_0^\infty r^2 p(r) dr$; using Eq. (1.1-14) for $p(r)$, we also get $\langle r^2 \rangle = 2b_0$.)

The hypergeometric function may be expanded in an infinite series:

$$R_r(\tau) = \frac{\pi}{2} b_0 \left[1 + \frac{1}{4} \rho^2(\tau) + \frac{1}{8} \rho^4(\tau) + \dots \right]. \quad (1.3-15)$$

Dropping terms beyond second degree,

$$R_r(\tau) \doteq \frac{\pi}{2} b_0 \left[1 + \frac{1}{4} \rho^2(\tau) \right]. \quad (1.3-16)$$

At $\tau=0$ this expression gives

$$R_r(0) = \frac{5\pi}{8} b_0 = 1.964b_0, \quad (1.3-17)$$

which differs from the true value of $2b_0$ by only 1.8%; thus Eq. (1.3-16) serves as a good approximation to the exact $R_r(\tau)$.

The power spectral density of the envelope can now be expressed as the Fourier transform of $R_r(\tau)$, using Eq. (1.3-16):

$$S_e(f) = \frac{\pi}{2} b_0 \int_{-\infty}^{\infty} \left[1 + \frac{1}{4} \rho^2(\tau) \right] e^{-i\omega\tau} d\tau. \quad (1.3-18)$$

$$= \frac{\pi}{2} b_0 \delta(f) + \frac{\pi}{8b_0} \int_{-\infty}^{\infty} \left[g^2(\tau) + h^2(\tau) \right] e^{-i\omega\tau} d\tau. \quad (1.3-19)$$

To evaluate this integral we first combine $g(\tau)$ and $h(\tau)$ into a complex quantity:

$$\phi(\tau) = g(\tau) + ih(\tau) = \frac{1}{2\pi} \int_{-\infty}^{\infty} F(\omega) e^{i\omega\tau} d\omega, \quad (1.3-20)$$

where $F(\omega)$ is a two-sided, real, usually even spectrum:

$$F(2\pi f) = S_i(f + f_c). \quad (1.3-21)$$

Then $g^2(\tau) + h^2(\tau) = \phi(\tau)\phi^*(\tau)$. Equation (1.3-20) indicates that the Fourier transform of $\phi(\tau)$ is $F(\omega)$; to get the transform of $\phi^*(\tau)$ we note that

$$\begin{aligned} \phi^*(\tau) &= \frac{1}{2\pi} \int_{-\infty}^{\infty} F^*(\omega) e^{-i\omega\tau} d\omega \\ &= \frac{-1}{2\pi} \int_{\infty}^{-\infty} F(-\omega) e^{i\omega\tau} d\omega \\ &= \frac{1}{2\pi} \int_{-\infty}^{\infty} F(\omega) e^{i\omega\tau} d\omega, \end{aligned} \tag{1.3-22}$$

Thus $\phi^*(\tau)$ has the same transform as $\phi(\tau)$. Applying the convolution theorem,

$$\int_{-\infty}^{\infty} \phi(\tau)\phi^*(\tau) e^{-i\omega\tau} d\tau = \frac{1}{2\pi} \int_{-\infty}^{\infty} F(y)F(y-\omega) dy,$$

or

$$\int_{-\infty}^{\infty} [g^2(\tau) + h^2(\tau)] e^{-i\omega\tau} d\tau = \frac{1}{2\pi} \int_{-\infty}^{\infty} F(y)F(y-\omega) dy. \tag{1.3-23}$$

The spectrum of the envelope is then

$$S_e(f) = \frac{\pi}{2} b_0 \delta(f) + \frac{1}{16b_0} \int_{-\infty}^{\infty} F(y)F(y-\omega) dy. \tag{1.3-24}$$

$S_e(f)$ is always positive, real, and even. The first term in Eq. (1.3-24) is just a dc component. The second term contains one band of width $4f_m$, centered at $f=0$. This band represents the continuous spectral content of the varying envelope. For positive frequencies it may be expressed as

$$S_0(f) = \frac{\pi}{8b_0} \int_{f_c-f_m}^{f_c+f_m-f} S_i(x)S_i(x+f) dx, \quad 0 < f < 2f_m. \tag{1.3-25}$$

1.3.3 Envelope Spectra of the Field Components

Using Eq. (1.3-25) we can now derive expressions for the baseband envelope spectral densities of the three electromagnetic field components, using Eqs. (1.2-11) to (1.2-13) for $S_i(f)$.

Electric field:

$$S_{0E_z}(f) = \frac{\pi b_0}{2\omega_m^2} \int_{f_c-f_m}^{f_c+f_m-f} \left\{ \left[1 - \left(\frac{x-f_c}{f_m} \right)^2 \right] \left[1 - \left(\frac{x+f-f_c}{f_m} \right)^2 \right] \right\}^{-1/2} dx. \tag{1.3-26}$$

This can be integrated exactly¹⁴ to give

$$S_{0E_z}(f) = \frac{b_0}{4\omega_m} K \left[\sqrt{1 - \left(\frac{f}{2f_m} \right)^2} \right], \tag{1.3-27}$$

where $K(x)$ is the complete elliptic integral of the first kind.

Magnetic field, x -component:

$$\begin{aligned} S_{0H_x}(f) &= \frac{2\pi b_{0H}}{\omega_m^2} \int_{f_c-f_m}^{f_c+f_m-f} \left\{ \left[1 - \left(\frac{x-f_c}{f_m} \right)^2 \right] \left[1 - \left(\frac{x+f-f_c}{f_m} \right)^2 \right] \right\}^{1/2} dx \\ &= \frac{4b_{0H}}{3\omega_m} \left\{ \left[1 + \left(\frac{f}{2f_m} \right)^2 \right] E \left[\sqrt{1 - \left(\frac{f}{2f_m} \right)^2} \right] \right. \\ &\quad \left. - 2 \left(\frac{f}{2f_m} \right)^2 K \left[\sqrt{1 - \left(\frac{f}{2f_m} \right)^2} \right] \right\}, \end{aligned} \tag{1.3-28}$$

where $E(x)$ is the complete elliptic integral of the second kind.

Magnetic field, y -component:

$$\begin{aligned}
 S_{0H_y}(f) &= \frac{2\pi b_{0H}}{\omega_m^2} \int_{f_c-f_m}^{f_c+f_m-f} \left\{ \left[1 - \left(\frac{x-f_c}{f_m} \right)^2 \right] \left[1 - \left(\frac{x+f-f_c}{f_m} \right)^2 \right] \right\}^{-1/2} \\
 &\quad \times \left(\frac{x-f_c}{f_m} \right)^2 \left(\frac{x+f-f_c}{f_m} \right)^2 dx \\
 &= \frac{b_{0H}}{\omega_m} \left\{ \left[1 + \frac{1}{3} \left(\frac{f}{f_m} \right)^2 \right] K \left[\sqrt{1 - \left(\frac{f}{2f_m} \right)^2} \right] \right. \\
 &\quad \left. - \frac{1}{3} \left[8 - \left(\frac{f}{f_m} \right)^2 \right] E \left[\sqrt{1 - \left(\frac{f}{2f_m} \right)^2} \right] \right\}. \tag{1.3-29}
 \end{aligned}$$

These spectra are shown in Figure 1.3-1. Experimental measurements of the spectrum of the electric field envelope¹⁵ in general show reasonably good agreement with the theoretical expression of Eq. (1.3-27). A modification to the original scattering model helps to explain some of the fine structure observed in the experimental spectra. In many actual cases the environment is such that a constant direct wave from the transmitter could be expected, as shown in Figure 1.3-2(a). This wave, arriving at an angle α_0 with respect to the mobile velocity vector, would experience a Doppler shift of $f_m \cos \alpha_0$. The resultant electric field spectrum density would appear as shown in Figure 1.3-2(b), and can be written

$$S'_{E_z}(f) = S_{E_z}(f) + B\delta(f - f_c - f_a), \tag{1.3-30}$$

where B is a weighting factor. The modified baseband output spectrum of the resulting envelope is then, using Eq. (1.3-25),

$$\begin{aligned}
 S'_{0E_z}(f) &= \frac{b_0}{b_0 + B} S_{0E_z}(f) \\
 &\quad + \frac{\pi B}{8(b_0 + B)} [S_{E_z}(f_c + f_a + f) + S_{E_z}(f_c + f_a - f)] + dc. \tag{1.3-31}
 \end{aligned}$$

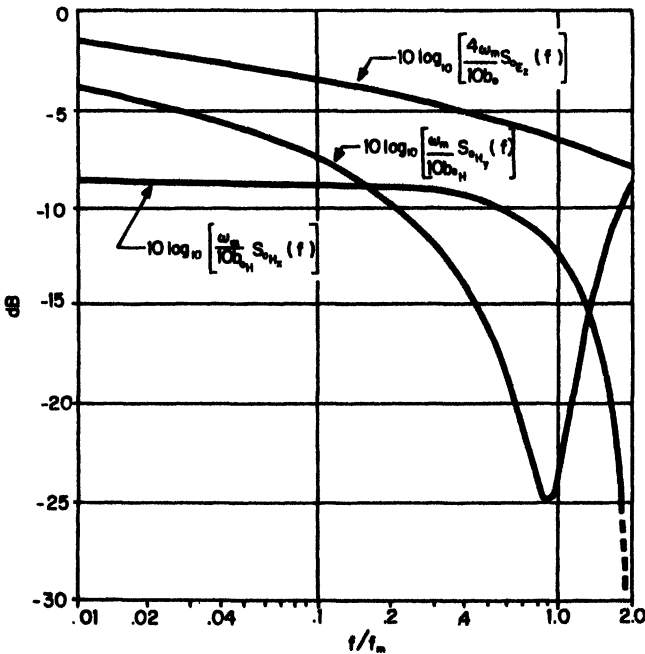


Figure 1.3-1 Baseband spectra of the field envelopes.

The ac part of the new spectrum is simply the original spectrum, $S_{0E}(f)$, plus a shifted and folded portion of the input spectrum, $S_{E}(f)$. The result will thus contain two new peaks, located at $f_m(1 \pm \cos \alpha_0)$, but will still cut off at $2f_m$, as before. Figure 1.3-2(c) shows an example of the modified spectrum for $\alpha = 60^\circ$. Two experimental spectra are shown in the solid curves of Figure 1.3-3,⁷ one with $\alpha_0 = 90^\circ$ and the other with $\alpha_0 = 0^\circ$. The dotted curves are taken from Eq. (1.3-31) with the constant B adjusted arbitrarily for best fit. The modified model gives the basic form of the experimental spectra, but there remain differences in detail. This is probably due to departures of $p(\alpha)$ from the assumed uniform distribution, and also to the fact that the process represented by the received signal is not truly stationary, as assumed, but contains slowly varying terms associated with gross changes in terrain features.

1.3.4 Level Crossing Rates

As illustrated in Figure 1.1-1 the signal envelope experiences very deep fades only occasionally; the shallower the fade the more frequently it is

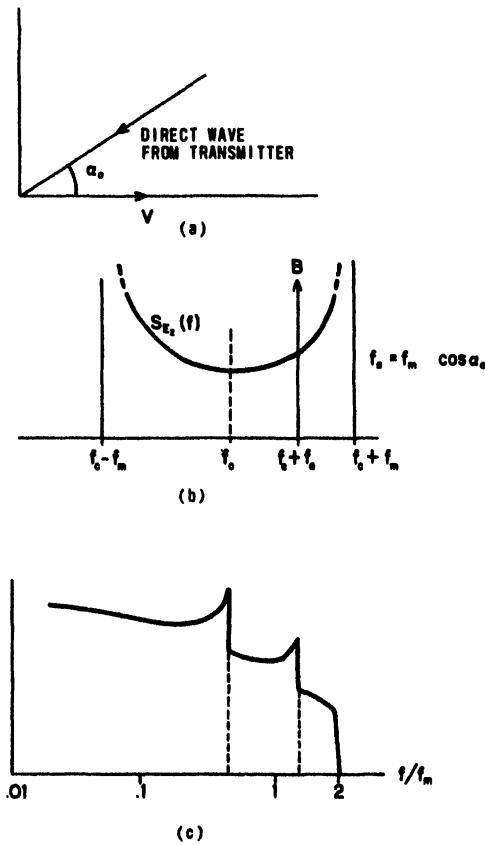


Figure 1.3-2 Effect of the addition of a direct wave from the transmitter on the envelope spectrum. (a) Geometry, (b), input spectrum, (c) spectrum of the envelope.

likely to occur. A quantitative expression of this property is the level crossing rate, N_R , which is defined as the expected rate at which the envelope crosses a specified signal level, R , in the positive direction. In general, it is given by⁸

$$N_R = \int_0^\infty \dot{r} p(R, \dot{r}) d\dot{r}, \tag{1.3-32}$$

where the dot indicates the time derivative and $p(R, \dot{r})$ is the joint density

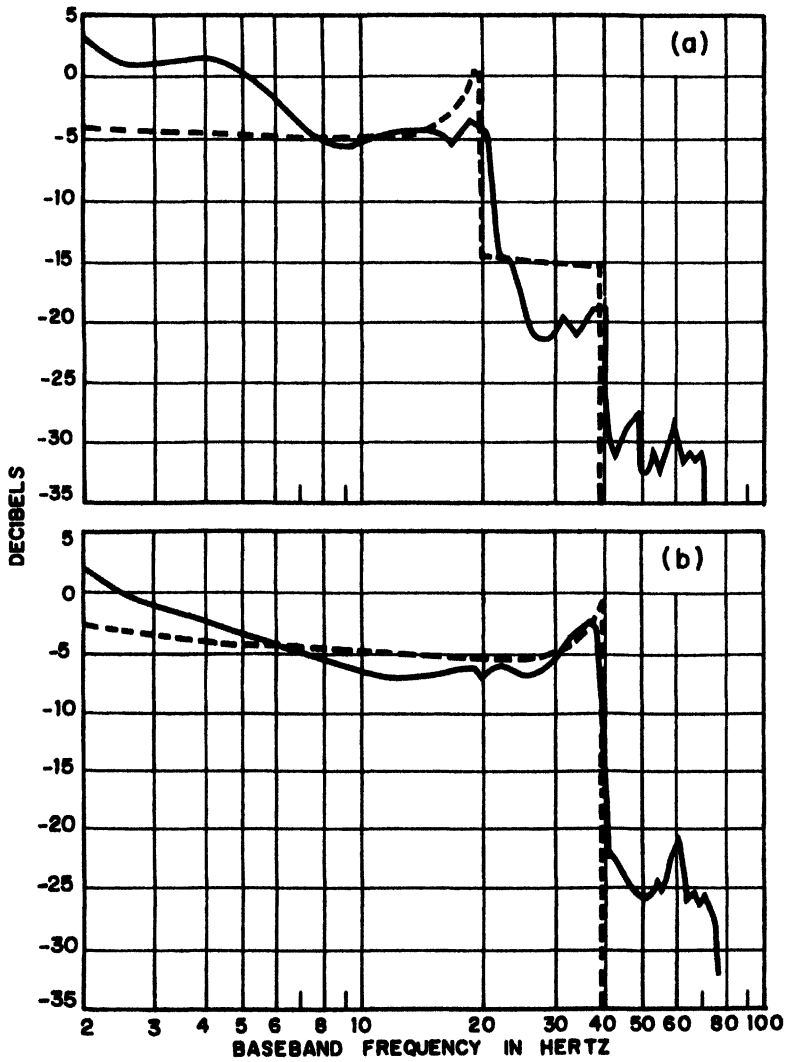


Figure 1.3-3 Comparison of theoretical (dashed) and experimental baseband spectra with direct wave from transmitter. (a) $\alpha_0 = 90^\circ$, (b) $\alpha_0 = 0^\circ$.

function of r and \dot{r} at $r=R$. Rice⁸ gives the joint density function in the four random variables $r, \dot{r}, \theta, \dot{\theta}$ of a Gaussian process for the case $b_1=0$:

$$p(r, \dot{r}, \theta, \dot{\theta}) = \frac{r^2}{4\pi^2 b_0 b_2} \exp \left[-\frac{1}{2} \left(\frac{r^2}{b_0} + \frac{\dot{r}^2}{b_2} + \frac{r^2 \dot{\theta}^2}{b_2} \right) \right], \quad (1.3-33)$$

where $\tan \theta = -T_s/T_c$. Integrating this expression over θ from 0 to 2π and $\dot{\theta}$ from $-\infty$ to $+\infty$ we get

$$p(r, \dot{r}) = \underbrace{\frac{r}{b_0} e^{-r^2/2b_0}}_{p(r)} \underbrace{\frac{1}{\sqrt{2\pi b_2}} e^{-\dot{r}^2/2b_2}}_{p(\dot{r})}. \quad (1.3-34)$$

Since $p(r, \dot{r}) = p(r)p(\dot{r})$, r and \dot{r} are independent and uncorrelated. Substituting Eq. (1.3-34) into Eq. (1.3-32) we get the level crossing rate:

$$\begin{aligned} N_R &= \frac{p(R)}{\sqrt{2\pi b_2}} \int_0^\infty \dot{r} e^{-\dot{r}^2/2b_2} d\dot{r} \\ &= \sqrt{\frac{b_2}{\pi b_0}} \rho e^{-\rho^2}, \end{aligned} \quad (1.3-35)$$

where

$$\rho = \frac{R}{\sqrt{\langle r^2 \rangle}} = \frac{R}{\sqrt{2b_0}} = \frac{R}{R_{\text{rms}}}. \quad (1.3-36)$$

Substituting the appropriate values of the moments, b_0 and b_2 , we get the expressions for the level crossing rates of the three field components*:

$$E_z: \quad N_R = \sqrt{2\pi} f_m \rho e^{-\rho^2}, \quad (1.3-37)$$

$$H_x: \quad N_R = \sqrt{\pi} f_m \rho e^{-\rho^2}, \quad (1.3-38)$$

$$H_y: \quad N_R = \sqrt{3\pi} f_m \rho e^{-\rho^2}. \quad (1.3-39)$$

*In case $b_1 \neq 0$:

$$N_R = \frac{\rho e^{-\rho^2}}{\sqrt{\pi b_0}} \sqrt{b_2 - \frac{b_1^2}{b_0}}.$$

These expressions are plotted in Figure 1.3-4 along with some measured values.¹ The rms level of E_z is crossed at a rate of $0.915 f_m$; for example, at $f = 1000$ MHz and $v = 60$ mi/hr, $f_m = 90$ Hz; thus $N_R = 82$ /sec at $\rho = 0$ dB. Lower signal levels are crossed less frequently, as shown by the curves. The maximum level crossing rate occurs at $\rho = -3$ dB.

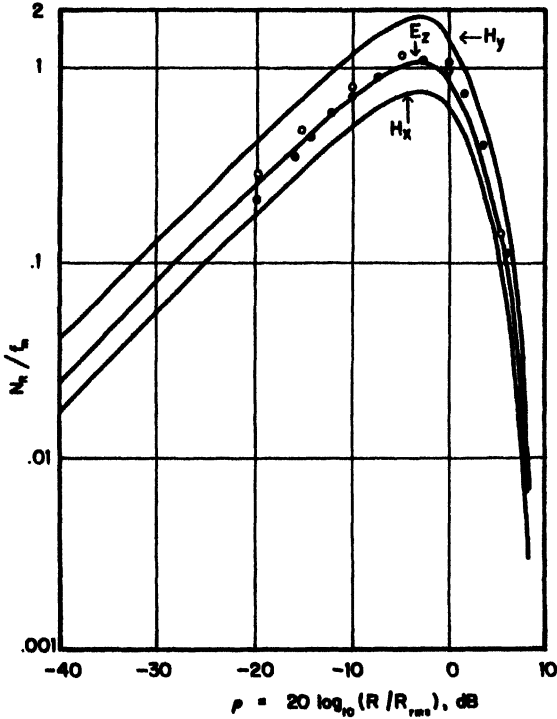


Figure 1.3-4 Normalized level crossing rates of the envelopes of the three field components. Measured values; O, 11,215 MHz, ●, 836 MHz (E_z).

1.3.5 Duration of Fades

The average duration of fades below $r = R$ is also of interest. Let τ_i be the duration of the i th fade. Then the probability that $r < R$ for a total time interval of length T is

$$P[r < R] = \frac{1}{T} \sum \tau_i. \tag{1.3-40}$$

The average fade duration is

$$\bar{\tau} = \frac{1}{TN_R} \sum \tau_i = \frac{1}{N_R} P[r < R], \quad (1.3-41)$$

$$P[r < R] = \int_0^R p(r) dr = 1 - e^{-\rho^2}, \quad (1.3-42)$$

so that

$$\bar{\tau} = \sqrt{\frac{\pi b_0}{b_2}} \frac{1}{\rho} (e^{\rho^2} - 1), \quad (1.3-43)$$

using Eq. (1.3-35) for N_R . Substituting the appropriate values of the moments, we get

$$E_z: \quad \bar{\tau} = \frac{e^{\rho^2} - 1}{\rho f_m \sqrt{2\pi}}, \quad (1.3-44)$$

$$H_z: \quad \bar{\tau} = \frac{e^{\rho^2} - 1}{\rho f_m \sqrt{\pi}}, \quad (1.3-45)$$

$$H_y: \quad \bar{\tau} = \frac{e^{\rho^2} - 1}{\rho f_m \sqrt{3\pi}}. \quad (1.3-46)$$

These expressions are shown in Figure 1.3-5, again with some measured values.¹

1.3.6 Envelope Autocorrelations and Cross Correlations of the Field Components

From the expressions for $g(\tau)$ and $h(\tau)$ the autocorrelation functions for the envelopes of the three field components may also be derived. In all three cases $h(\tau) = 0$; thus $\rho^2(\tau) = g^2(\tau)/b_0^2$. Using the approximate expression for the envelope autocorrelation of Eq. (1.3-16) we can get the autocovariance function (mean value removed). For a stationary process $r(t)$,

$$L(\tau) \equiv \langle [r(t) - \langle r \rangle][r(t + \tau) - \langle r \rangle] \rangle = R(\tau) - \langle r \rangle^2. \quad (1.3-47)$$

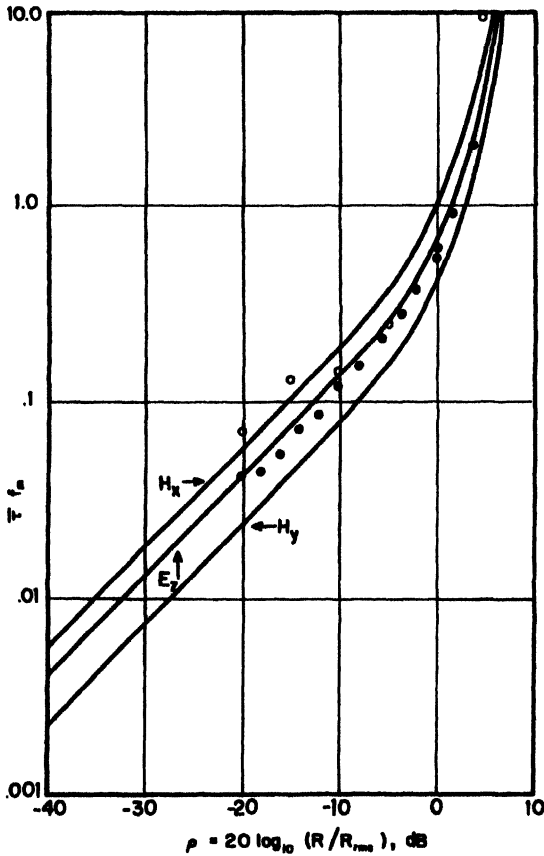


Figure 1.3-5 Normalized durations of fade of the envelopes of the three field components. Measured values: O, 11,215 MHz, ●, 836 MHz (E_z).

In our case $p(r) = (r/b_0)e^{-r^2/2b_0}$; thus

$$\langle r \rangle = \frac{1}{b_0} \int_0^\infty r^2 e^{-r^2/2b_0} dr = \sqrt{\frac{\pi b_0}{2}} \tag{1.3-48}$$

Substituting in Eq. (1.3-16),

$$L_e(\tau) \doteq \frac{\pi b_0}{8} \rho^2(\tau) = \frac{\pi}{8b_0} g^2(\tau). \tag{1.3-49}$$

For the three field components,

$$E_z: \quad L_e(\tau) = \frac{\pi}{8} b_0 J_0^2(\omega_m \tau), \quad (1.3-50)$$

$$H_x: \quad L_e(\tau) = \frac{\pi}{8} b_{0H} [J_0(\omega_m \tau) + J_2(\omega_m \tau)]^2, \quad (1.3-51)$$

$$H_y: \quad L_e(\tau) = \frac{\pi}{8} b_{0H} [J_0(\omega_m \tau) - J_2(\omega_m \tau)]^2. \quad (1.3-52)$$

The cross-covariance functions between the envelopes of the three field components are also of interest. We have shown earlier that E_z and H_x are uncorrelated for any value of τ if $p(\alpha)$ is even, and likewise for H_x and H_y . Thus the envelopes of these fields will also be uncorrelated. Using the series expressions for E_z and H_y , it can be shown that the correlation between the envelopes of E_z and H_y is given in terms of a hypergeometric function if $p(\alpha) = 1/2\pi$:

$$R_e(\tau) = \frac{\pi}{2} \sqrt{b_0 b_{0H}} F\left[-\frac{1}{2}, -\frac{1}{2}; 1; 2J_1^2(\omega_m \tau)\right], \quad (1.3-53)$$

which can be approximated to better than 1% accuracy for any value of τ by

$$R_e(\tau) \doteq \frac{\pi}{2} \sqrt{b_0 b_{0H}} [1 + \frac{1}{2} J_1^2(\omega_m \tau)]. \quad (1.3-54)$$

The cross-covariance function is then

$$L_e(\tau) \doteq \frac{\pi}{4} \sqrt{b_0 b_{0H}} J_1^2(\omega_m \tau). \quad (1.3-55)$$

These four envelope covariances, Eqs. (1.3-50)–(1.3-52) and (1.3-55), are shown in Figure 1.3-6. (the envelope covariances for $E_z H_x$ and $H_x H_y$ are zero as pointed out earlier, and thus are not shown in Figure 1.3-6.) These would be the functions measured in the mobile as a function of time while it moves with uniform velocity; alternatively, they can be regarded as spatial correlations by setting $\zeta = v\tau$; thus $\omega_m \tau = \beta \zeta / \lambda$. This equivalence between time and spatial correlations is important and should be noted, since it will be used in space diversity calculations and other applications.

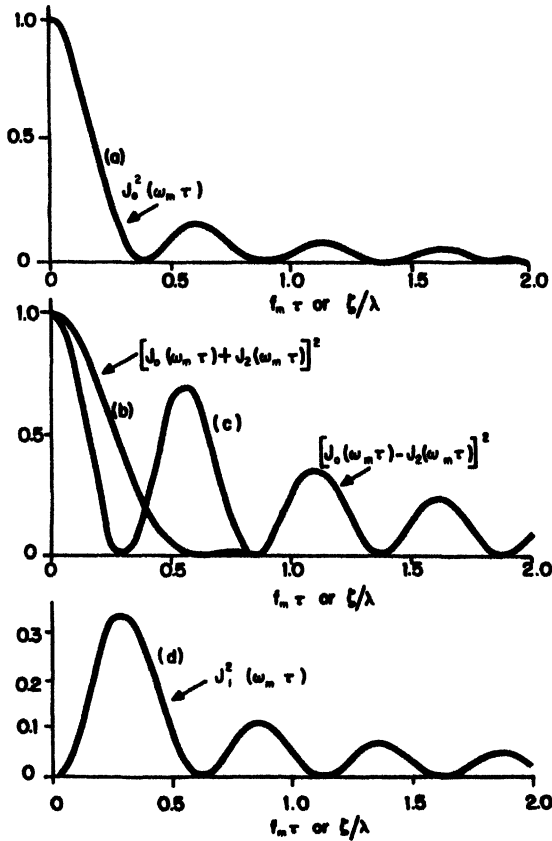


Figure 1.3-6 Covariance functions of various field envelopes. (a) $|E_x|$, (b) $|H_x|$, (c) $|H_y|$, (d) cross-covariance of $|E_x|$ and $|H_y|$.

1.4 RANDOM FREQUENCY MODULATION

1.4.1 Probability Distribution of Random FM

The time-varying nature of the in-phase and quadrature components of the fading signal means that the apparent frequency of the signal varies with time in a random manner; that is, the signal exhibits random frequency modulation. The characteristics of this random FM can be most easily described in terms of its probability distributions and power spectrum. The probability density of θ can be easily obtained from

$p(r, \dot{r}, \theta, \dot{\theta})$ by integrating over $r, \dot{r},$ and θ . Using Eq. (1.3-33),

$$\begin{aligned}
 p(\dot{\theta}) &= \frac{1}{4\pi^2 b_0 b_2} \int_0^\infty dr \int_{-\infty}^\infty d\dot{r} \int_0^{2\pi} d\theta \\
 &\quad \times r^2 \exp \left[-\frac{1}{2} \left(\frac{r^2}{b_0} + \frac{\dot{r}^2}{b_2} + \frac{r^2 \dot{\theta}^2}{b_2} \right) \right] \\
 &= \frac{1}{2} \sqrt{\frac{b_0}{b_2}} \left(1 + \frac{b_0}{b_2} \dot{\theta}^2 \right)^{-3/2}. \tag{1.4-1}
 \end{aligned}$$

From the expression for $p(\dot{\theta})$ we can deduce the somewhat surprising result that the mean square value of the random FM is infinite:

$$\begin{aligned}
 \langle \dot{\theta}^2 \rangle &= \int_{-\infty}^\infty \dot{\theta}^2 p(\dot{\theta}) d\dot{\theta} \\
 &= \frac{b_0}{b_2} \left[-1 + \lim_{\theta \rightarrow \infty} \log \left(2\dot{\theta} \sqrt{\frac{b_0}{b_2}} \right) \right] = \infty.* \tag{1.4-2}
 \end{aligned}$$

In actual FM receivers, of course, the discriminator or audio amplifiers will limit at some value of frequency deviation. With this assumption it then becomes possible to calculate the rms baseband noise due to the random FM, as is shown in Chapter 4.

For the E_z field $b_2/b_0 = \omega_m^2/2$, using Eq. (1.3-6), thus $p(\dot{\theta})$ can be written:

$$E_z: p(\dot{\theta}) = \frac{1}{\omega_m \sqrt{2}} \left[1 + 2 \left(\frac{\dot{\theta}}{\omega_m} \right)^2 \right]^{-3/2}. \tag{1.4-3}$$

*When log appears without subscript, the natural log is assumed.

The cumulative distribution function is

$$\begin{aligned}
 P[\dot{\theta} < \dot{\theta}_0] &= \frac{1}{2} \sqrt{\frac{b_0}{b_2}} \int_{-\infty}^{\dot{\theta}_0} \left(1 + \frac{b_0}{b_2} \dot{\theta}^2\right)^{-3/2} d\dot{\theta} \\
 &= \frac{1}{2} \left[1 + \sqrt{\frac{b_0}{b_2}} \dot{\theta}_0 \left(1 + \frac{b_0}{b_2} \dot{\theta}_0^2\right)^{-1/2} \right], \quad (1.4-4)
 \end{aligned}$$

$$E_z: P[\dot{\theta} < \dot{\theta}_0] = \frac{1}{2} \left[1 + \sqrt{2} \frac{\dot{\theta}_0}{\omega_m} \left(1 + 2 \frac{\dot{\theta}_0^2}{\omega_m^2}\right)^{-1/2} \right]. \quad (1.4-5)$$

These probability functions are similar for the other two field components, differing only in scale. Equations (1.4-3) and (1.4-5) are shown in Figure 1.4-1. Note that, in contrast to the sharply defined power spectrum of the signal (Figure 1.2-1), there is a nonzero probability of finding its frequency at any value, although the larger excursions occur only rarely since they are associated with the deeper fades of the signal. This can be seen by examining the probability density function of θ conditioned on the signal level R :

$$p(\dot{\theta}|R) = \frac{p(\dot{\theta}, R)}{p(R)} = \frac{R}{\sqrt{2\pi b_2}} e^{-R^2 \dot{\theta}^2 / 2b_2}. \quad (1.4-6)$$

For fixed R this is a Gaussian distribution with standard deviation $\sqrt{b_2}/R$. Thus as R decreases (deep fades) the frequency deviations of interest increase proportionately. If $R = R_{rms} = \sqrt{2b_0}$ the significant deviations occupy a bandwidth approximately equal to ω_m in the case of E_z ; for a 20-dB fade the bandwidth is ten times greater.

1.4.2 Power Spectrum of Random FM

The power spectrum of $\dot{\theta}$ may be derived by conventional methods. The

autocorrelation function of $\dot{\theta}$ is given by Rice⁸:

$$R_{\dot{\theta}}(\tau) = \langle \dot{\theta}(t)\dot{\theta}(t+\tau) \rangle$$

$$= -\frac{1}{2} \left\{ \left[\frac{g'(\tau)}{g(\tau)} \right] - \left[\frac{g''(\tau)}{g(\tau)} \right] \right\} \log \left\{ 1 - \left[\frac{g(\tau)}{g(0)} \right]^2 \right\}. \quad (1.4-7)$$

Then the power spectrum is the Fourier transform of $R_{\dot{\theta}}(\tau)$:

$$S_{\dot{\theta}}(f) = \int_{-\infty}^{\infty} R_{\dot{\theta}}(\tau) e^{-i\omega\tau} d\tau = 4 \int_0^{\infty} R_{\dot{\theta}}(\tau) \cos \omega\tau d\tau, \quad (1.4-8)$$

where a factor of 2 introduced into the second factor since we are only interested in positive frequencies.

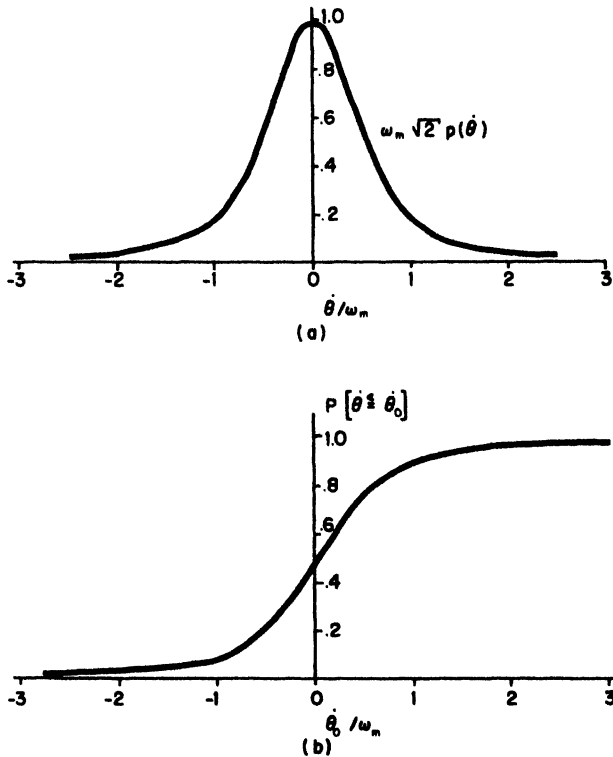


Figure 1.4-1 Probability functions for the random frequency modulation, $\dot{\theta}$, of the electric field. (a) Probability density, (b) cumulative distribution.

Considering now the E_z field for the case $p(\alpha) = 1/2\pi$, the values of $g(\tau)$ and its derivatives can be obtained from Eq. (1.3-7):

$$\frac{g(\tau)}{g(0)} = J_0(u), \quad u = \omega_m \tau,$$

$$\frac{g'(\tau)}{g(\tau)} = -\omega_m \frac{J_1(u)}{J_0(u)}, \quad (1.4-9)$$

$$\frac{g''(\tau)}{g(\tau)} = \omega_m^2 \left[\frac{J_1(u)}{u J_0(u)} - 1 \right],$$

and

$$R_\theta(\tau) = \frac{\omega_m^2}{2J_0^2(u)} \left[\frac{J_0(u)J_1(u)}{u} - J_0^2(u) - J_1^2(u) \right]$$

$$\times \log[1 - J_0^2(u)]. \quad (1.4-10)$$

The integration of Eq. (1.4-8) is then carried out by separating the range of integration into parts and making the appropriate approximations for the Bessel functions and the logarithm.

Region 1:

$$0 < \tau < \tau_A = \frac{1}{4\omega_m}, \quad J_0(u) \doteq 1 - \left(\frac{u}{2}\right)^2, \quad J_1(u) \doteq \frac{u}{2}.$$

$$S_1(f) \doteq -\omega_m \int_0^{\omega_m \tau_A} \log\left(\frac{u^2}{2}\right) \cos\left(\frac{\omega}{\omega_m} u\right) du$$

$$= -\frac{\omega_m^2}{\omega} \left[\log\left(\frac{\omega_m^2 \tau_A^2}{2}\right) \sin(\omega \tau_A) - 2S_i(\omega \tau_A) \right], \quad (1.4-11)$$

where $S_i(\omega \tau_A)$ is the sine integral function.

Region 3:

$$\tau_B < \tau < \infty: \quad \log(1 - J_0^2) \doteq -J_0^2(u), \quad \tau_B \sim \frac{10}{\omega_m},$$

$$J_0(u) \sim \sqrt{\frac{2}{\pi u}} \cos\left(u - \frac{\pi}{4}\right),$$

$$J_1(u) \sim \sqrt{\frac{2}{\pi u}} \sin\left(u - \frac{\pi}{4}\right).$$

$$\begin{aligned} S_3(f) &= \frac{8\omega_m}{\pi} \int_{\omega_m \tau_B}^{\infty} \left[\frac{1}{2u} + \frac{\cos(2u)}{(2u)^2} \right] \cos\left(\frac{\omega}{\omega_m} u\right) du \\ &= \frac{2\omega_m}{\pi} \left[\frac{\cos(2\omega_m \tau_B) \cos(\omega \tau_B)}{\omega_m \tau_B} + \left(1 + \frac{\omega}{2\omega_m}\right) S_i(2\omega_m \tau_B + \omega \tau_B) \right. \\ &\quad \left. + \left(1 - \frac{\omega}{2\omega_m}\right) S_i(|2\omega_m \tau_B - \omega \tau_B|) - 2C_i(\omega \tau_B) \right. \\ &\quad \left. - \frac{\pi}{2} \left(1 + \frac{\omega}{2\omega_m} + \left|1 - \frac{\omega}{2\omega_m}\right|\right) \right]. \end{aligned} \tag{1.4-12}$$

Region 2: $\tau_A < \tau < \tau_B$. $S_2(f)$ must be evaluated by numerical integration. As ω approaches zero the spectrum has a logarithmic singularity due to the term $C_i(\omega \tau_B)$ in Eq. (1.4-12):

$$S_\theta(f) \rightarrow -\frac{4\omega_m}{\pi} \log(k\omega), \quad k = \text{a constant.}$$

The spectrum $S_\theta(f) = S_1(f) + S_2(f) + S_3(f)$ is shown in Figure 1.4-2. Above $\omega = 2\omega_m$ the spectrum falls as $1/f$; thus $2\omega_m$ may be regarded as an approximate cutoff frequency. Note that this is the same as the cutoff frequency of the envelope spectra (Figure 1.3-1).

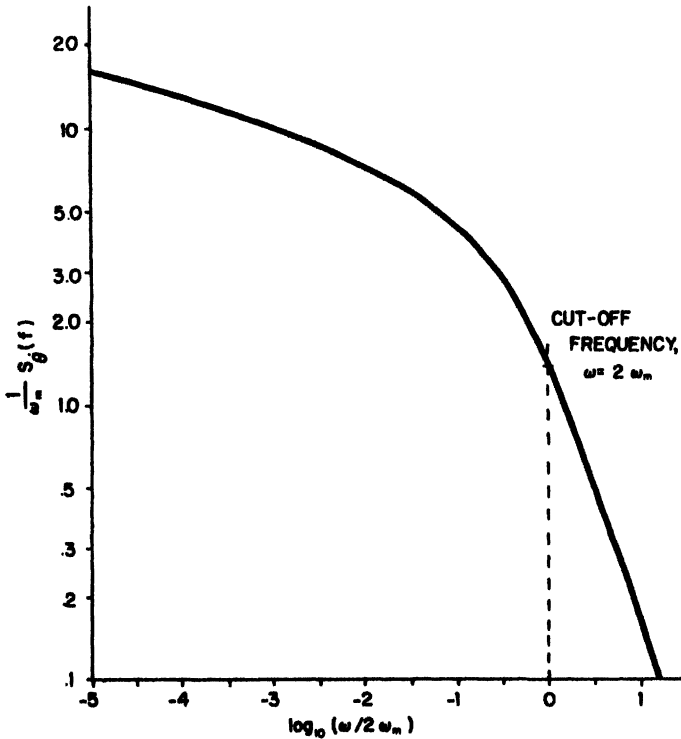


Figure 1.4-2 One-sided power spectrum of the instantaneous frequency, $\dot{\theta}$, of the E_z field.

Using Watson's lemma one can obtain the asymptotic form, as f approaches infinity, of the power spectrum of the random FM for an arbitrary Doppler spectrum¹⁶:

$$\lim_{f \rightarrow \infty} S_{\dot{\theta}}(f) \sim \left(\frac{b_2}{b_0} - \frac{b_1^2}{b_0^2} \right) f^{-1}, \tag{1.4-13}$$

where b_0, b_1, b_2 are defined in Eq. (1.3-4). For low vehicle speeds and low carrier frequencies (e.g., 60 mph at UHF), the asymptotic form given here is accurate over the audio band from 300 to 3000 Hz.

1.5 COHERENCE BANDWIDTH

The characteristics of a single-frequency signal transmitted over the

mobile radio propagation path have so far been explained on the basis of a fairly simple model. The only required knowledge was the angular distribution of the incident power, $p(\alpha)$, assumed to be carried by a large number of plane waves of random amplitudes, phases, and arrival angles. When we turn to questions concerning the statistics of several signals of different frequencies transmitted over the path, however, the model must be elaborated to include explicitly the fact that the path lengths of the constituent waves are different. The different path lengths give rise to different propagation time delays, of course. Typical spreads in time delays range from a fraction of a microsecond to many microseconds, depending on the type of environment. The longer delay spreads are usually found in metropolitan areas like New York City that contain many large buildings, whereas the shorter delay spreads are usually associated with suburban areas. In the latter the building structures are generally more uniform, consisting of one- or two-story houses.

The existence of the different time delays in the various waves that make up the total field causes the statistical properties of two signals of different frequencies to become essentially independent if the frequency separation is large enough. The maximum frequency difference for which the signals are still strongly correlated is called the coherence bandwidth of the mobile radio transmission path.

Besides providing a more complete physical model of the mobile transmission path, the study of the delay spreads and coherence bandwidth will be useful in assessing the performance and limitations of different modulation and diversity reception schemes, as we will see in later chapters.

1.5.1 Mathematical Model

We will now proceed to develop a mathematical model that includes the time delays explicitly. If a single signal of frequency ω is transmitted to the mobile unit, we assume the received field is the sum of a number of waves, as before:

$$E_z(\omega, t) = E_0 \sum_{n=1}^N \sum_{m=1}^M C_{nm} \cos(\omega t + \omega_n t - \omega T_{nm}). \quad (1.5-1)$$

In this representation the n th wave at an arrival angle α_n is composed of M waves with propagation delay times T_{nm} . All of these M waves experience the same Doppler shift, $\omega_n = \beta v \cos \alpha_n$.^{*} The amplitude coefficients C_{nm}

^{*}The Frontispiece, supplied by Cox (*IEEE Proc. Lett.*, April, 1973), gives a vivid illustration of this model.

have been redefined to indicate the power associated with each individual wave:

$$C_{nm}^2 = G(\alpha_n)p(\alpha_n, T_{nm})d\alpha dT. \tag{1.5-2}$$

As before, $G(\alpha)$ is the horizontal directivity pattern of the receiving antenna. We interpret $p(\alpha, T)d\alpha dT$ to mean the fraction of the incoming power within $d\alpha$ of the angle α and within dT of the time T , in the limit with N and M very large.

We assume that the α_n and T_{nm} remain constant for motion of the mobile over distances of several tens of wavelengths and that they are frequency independent. It also seems reasonable that the difference between any two phase angles, represented by $\omega T_{ij} - \omega T_{nm}$, is much greater than 2π for $i \neq n, j \neq m$. At UHF frequencies and above, $\omega > 2\pi \times 10^9$; thus for $(T_{ij} - T_{nm})$ on the order of 0.1 to 10 μ sec (the delay spread), the phase difference is on the order of several hundred times 2π , at least.

We consider the random process $E_z(\omega, t)$ to consist of sample functions corresponding to separate runs made by the mobile on the same section of street, and assume the phases $\omega_n t - \omega T_{nm}$ of the individual waves in the different sample functions are uniformly distributed independent random variables. The process $E_z(\omega, t)$ is then wide-sense stationary with respect to ensemble averages. It is not stationary with respect to time averages, however, and thus is nonergodic. But the difference between time and ensemble averages decreases as the number of waves becomes large; thus the statistical properties will be computed on the basis of ensemble averages. The results will eventually be compared with corresponding values derived from experiments, in which averages with time are usually used. The extent to which theory and experiment agree will govern the degree of confidence we place in the model.

To investigate the coherence bandwidth we will study the statistics and correlation properties of two signals received at frequencies ω_1 and ω_2 , and, in particular, of their envelopes and phases. Only the E_z field will be explicitly treated; corresponding results can be easily derived for H_x and H_y by defining an appropriate antenna pattern as in Section 1.2. We start by writing the field at the two frequencies in terms of narrow-band in-phase and quadrature components:

$$\begin{aligned} \text{At } \omega_1: \quad E_z(\omega_1, t) &= x_1(t) \cos \omega_1 t - x_2(t) \sin \omega_1 t, \\ \text{At } \omega_2: \quad E_z(\omega_2, t) &= x_3(t) \cos \omega_2 t - x_4(t) \sin \omega_2 t. \end{aligned} \tag{1.5-3}$$

For large enough N and M the $x_i(t)$ are Gaussian random processes (by

the Central Limit Theorem), and are jointly Gaussian.

They are expressed as

$$\begin{aligned} x_2^1(t) &= E_0 \sum_{n,m} C_{nm} \begin{Bmatrix} \cos \\ \sin \end{Bmatrix} (\omega_n t - \omega_1 T_{nm}), \\ x_4^3(t) &= E_0 \sum_{n,m} C_{nm} \begin{Bmatrix} \cos \\ \sin \end{Bmatrix} (\omega_n t - \omega_2 T_{nm}). \end{aligned} \quad (1.5-4)$$

We will be interested in correlation properties as a function of both time delay, τ , and frequency separation $s = \omega_2 - \omega_1$. Let us define the four random variables x_1, x_2, x_3, x_4 for fixed time t as follows:

$$\begin{aligned} x_1 &\stackrel{\Delta}{=} x_1(t), & x_2 &\stackrel{\Delta}{=} x_2(t), \\ x_3 &\stackrel{\Delta}{=} x_3(t + \tau), & x_4 &\stackrel{\Delta}{=} x_4(t + \tau). \end{aligned} \quad (1.5-5)$$

The envelopes and phases are then defined by

$$x_2^1 = \begin{Bmatrix} r_1 \cos \theta_1 \\ r_1 \sin \theta_1 \end{Bmatrix}, \quad x_4^3 = \begin{Bmatrix} r_2 \cos \theta_2 \\ r_2 \sin \theta_2 \end{Bmatrix}. \quad (1.5-6)$$

The statistical properties will depend on moments of the type $\langle x_i x_j \rangle$, where the brackets refer to ensemble averages. The moments are evaluated from the series expansion of Eq. (1.5-4):

$$\langle x_1^2 \rangle = E_0^2 \sum_{n,m,p,q} \langle C_{nm} C_{pq} \cos(\omega_n t - \omega_1 T_{nm}) \cos(\omega_p t - \omega_1 T_{pq}) \rangle. \quad (1.5-7)$$

The average will vanish unless $n = p$ and $m = q$, which gives

$$\langle x_1^2 \rangle = \frac{E_0^2}{2} \sum_{n,m} C_{nm}^2 = b_0 \sum_{n,m} G(\alpha_n) p(\alpha_n, T_{nm}) d\alpha dT. \quad (1.5-8)$$

In the limit as $N, M \rightarrow \infty$:

$$\langle x_1^2 \rangle = b_0 \int_0^{2\pi} G(\alpha) d\alpha \int_0^\infty p(\alpha, T) dT. \quad (1.5-9)$$

But, by definition,

$$\int_0^\infty p(\alpha, T) dT = p(\alpha); \quad (1.5-10)$$

thus

$$\langle x_1^2 \rangle = b_0 \int_0^{2\pi} G(\alpha) p(\alpha) d\alpha. \tag{1.5-11}$$

By similar arguments we can show

$$\langle x_1^2 \rangle = \langle x_2^2 \rangle = \langle x_3^2 \rangle = \langle x_4^2 \rangle, \tag{1.5-12}$$

$$\langle x_1 x_2 \rangle = \langle x_3 x_4 \rangle = 0, \tag{1.5-13}$$

$$\begin{aligned} \langle x_1 x_3 \rangle &= \langle x_2 x_4 \rangle \\ &= b_0 \int_0^{2\pi} G(\alpha) d\alpha \int_0^\infty p(\alpha, T) \cos(\beta v r \cos \alpha - sT) dT, \end{aligned} \tag{1.5-14}$$

$$\begin{aligned} \langle x_1 x_4 \rangle &= -\langle x_2 x_3 \rangle \\ &= b_0 \int_0^{2\pi} G(\alpha) d\alpha \int_0^\infty p(\alpha, T) \sin(\beta v r \cos \alpha - sT) dT. \end{aligned} \tag{1.5-15}$$

Using the general expression (Ref. 9, p. 255) for the joint density of the four Gaussian variables x_1, \dots, x_4 and applying the transformation of variables of Eq. (1.5-6), we get the joint density of the envelopes and phases:

$$\begin{aligned} p(r_1, r_2, \theta_1, \theta_2) &= \frac{r_1 r_2}{(2\pi\mu)^2 (1-\lambda^2)} \\ &\times \exp \left[-\frac{r_1^2 + r_2^2 - 2r_1 r_2 \lambda \cos(\theta_2 - \theta_1 - \phi)}{2\mu(1-\lambda^2)} \right], \end{aligned} \tag{1.5-16}$$

where

$$\tan \phi = \frac{\mu_2}{\mu_1}, \quad \lambda^2 = \frac{\mu_1^2 + \mu_2^2}{\mu^2}, \tag{1.5-17}$$

$$\mu = \langle x_1^2 \rangle, \quad \mu_1 = \langle x_1 x_3 \rangle, \quad \mu_2 = \langle x_1 x_4 \rangle. \tag{1.5-18}$$

All of the statistical properties of interest can now be derived from the four fold joint density function of Eq. (1.5-16) provided an explicit form

for $G(\alpha)$ and $p(\alpha, T)$ is known. Interpretation of some measured data^{7, 17, 18} indicates that an exponential distribution of the delay spreads is a good approximation. If we further assume a uniform distribution in angle of the incident power, the function $p(\alpha, T)$ can be expressed as

$$p(\alpha, T) = \frac{1}{2\pi\sigma} e^{-T/\sigma}, \quad (1.5-19)$$

where σ is a measure of the time delay spread.

With this assumption, and the additional one of no antenna directivity so that $G(\alpha) = 1$, the quantities in Eqs. (1.5-17)–(1.5-18) may be worked out with the help of Eqs. (1.5-11)–(1.5-14):

$$\begin{aligned} \mu &= b_0, & \mu_1 &= b_0 \frac{J_0(\omega_m \tau)}{1 + s^2 \sigma^2}, & \mu_2 &= -s\sigma\mu_1. \end{aligned} \quad (1.5-20)$$

$$\tan \phi = -s\sigma, \quad \lambda^2 = \frac{J_0^2(\omega_m \tau)}{1 + s^2 \sigma^2}.$$

1.5.2 Envelope Correlation as a Function of Frequency Separation

The correlation of the envelopes of the signals at the two frequencies may now be calculated. We have

$$R_e(s, \tau) = \langle r_1 r_2 \rangle = \int_0^\infty \int_0^\infty r_1 r_2 p(r_1, r_2) dr_1 dr_2. \quad (1.5-21)$$

We can get $p(r_1, r_2)$ by integrating Eq. (1.5-16):

$$\begin{aligned} p(r_1, r_2) &= \int_0^{2\pi} \int_0^{2\pi} p(r_1, r_2, \theta_1, \theta_2) d\theta_1 d\theta_2 \\ &= \frac{r_1 r_2}{\mu^2(1-\lambda^2)} \exp \left[-\frac{r_1^2 + r_2^2}{2\mu(1-\lambda^2)} \right] I_0 \left(\frac{r_1 r_2}{\mu} \frac{\lambda}{1-\lambda^2} \right), \end{aligned} \quad (1.5-22)$$

where $I_0(x)$ is the modified Bessel function of zero order.

Substituting Eq. (1.5-22) into Eq. (1.5-21) the integration may be carried out exactly¹⁴ to give

$$R_e(s, \tau) = \frac{\pi}{2} b_0 F(-\frac{1}{2}, -\frac{1}{2}; 1; \lambda^2), \quad (1.5-23)$$

which may also be expressed as¹⁴

$$R_e(s, \tau) = b_0(1 + \lambda)E\left(\frac{2\sqrt{\lambda}}{1 + \lambda}\right), \tag{1.5-24}$$

where $E(x)$ is the complete elliptic integral of the second kind. The expansion of the hypergeometric function yields a good approximation to Eq. (1.5-23):

$$R_e(s, \tau) \doteq \frac{\pi}{2} b_0 \left(1 + \frac{\lambda^2}{4}\right). \tag{1.5-25}$$

We know that $\langle r_1 \rangle = \langle r_2 \rangle = \sqrt{\frac{1}{2}\pi b_0}$ from Eq. (1.3-48) and also that $\langle r_1^2 \rangle = \langle r_2^2 \rangle = 2b_0$ from Eq. (1.3-14); thus the envelope correlation coefficient

$$\rho_e(s, \tau) = \frac{R_e(s, \tau) - \langle r_1 \rangle \langle r_2 \rangle}{\sqrt{[\langle r_1^2 \rangle - \langle r_1 \rangle^2][\langle r_2^2 \rangle - \langle r_2 \rangle^2]}}$$

becomes

$$\begin{aligned} \rho_e(s, \tau) &= \frac{(1 + \lambda)E\left(\frac{2\sqrt{\lambda}}{1 + \lambda}\right) - \frac{\pi}{2}}{2 - \frac{\pi}{2}} \\ &\doteq \lambda^2 = \frac{J_0^2(\omega_m \tau)}{1 + s^2 \sigma^2}. \end{aligned} \tag{1.5-26}$$

We see from this expression that the correlation between the envelopes decreases with increasing frequency separation s , as one would expect. One measure of coherence bandwidth corresponds to the frequency separation when the envelope correlation is 0.5. With $\tau = 0$ this occurs when $s\sigma = 1$; thus the coherence bandwidth is equal to $1/2\pi\sigma$. Equation (1.5-26) with $\tau = 0$ is plotted in Figure 1.5-1 for values of σ in the range $\frac{1}{4}$ to $\frac{3}{4}$ μ sec. Also shown are a few measurements made in 1961 by Ossanna and Hoffman* in a suburban area at 836 MHz. A delay spread on the order of $\frac{1}{4}$ μ sec appears to be appropriate in this case, corresponding to a coherence bandwidth of about 640 KHz. Measurements of the delay spread using a more direct pulse-type technique¹⁹ tend to substantiate this value of time

*Bell Telephone Laboratories, unpublished work.

delay spread for suburban areas. Other delay distributions besides the exponential one of Eq. (1.5-18) could also be considered,⁶ but they do not appreciably change the shape of the curves in Figure 1.5-1.

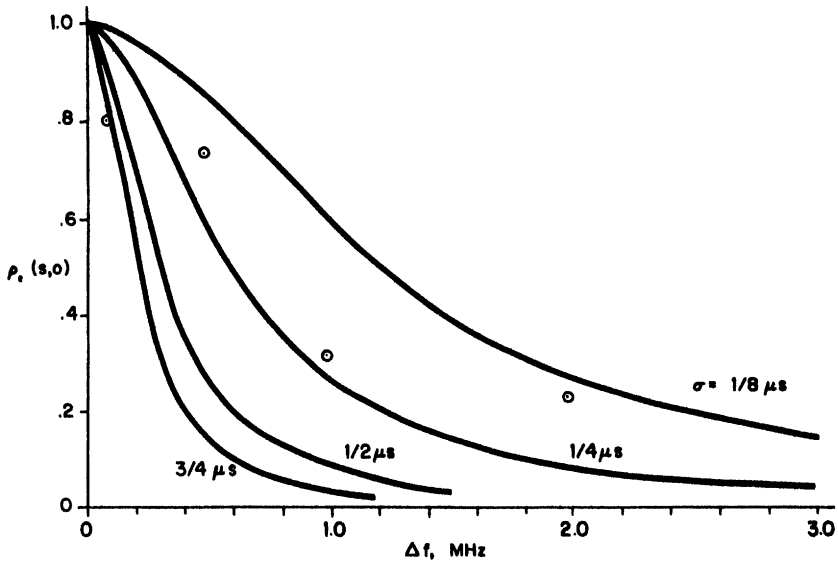


Figure 1.5-1 Envelope correlation of signals received at two frequencies for different time delay spreads, σ . Solid curves are theoretical for an exponential delay distribution. \circ -measurements at 836 MHz in a suburban environment.

1.5.3 Phase Correlation as a Function of Frequency Separation

The statistics of the phases of the two signals are also of interest. (Note that we mean the phase angles of the signal phasors, θ_1 and θ_2 , not the radio frequency phases.) One property is the correlation of the two phases:

$$R_\theta(s, \tau) = \langle \theta_1, \theta_2 \rangle = \int_0^{2\pi} \int_0^{2\pi} \theta_1, \theta_2 p(\theta_1, \theta_2) d\theta_1 d\theta_2. \quad (1.5-27)$$

Again we can obtain $p(\theta_1, \theta_2)$ by integrating Eq. (1.5-16):

$$p(\theta_1, \theta_2) = \int_0^\infty \int_0^\infty p(r_1, r_2, \theta_1, \theta_2) dr_1 dr_2.$$

The integration is straightforward, using known integrals of error functions²⁰ to obtain

$$p(\theta_1, \theta_2) = \frac{1 - \lambda^2}{4\pi^2} \frac{\sqrt{1 - B^2} + B \cos^{-1}(-B)}{(1 - B^2)^{3/2}}, \quad (1.5-28)$$

where

$$B = \lambda \cos(\theta_2 - \theta_1 - \phi), \quad 0 < \cos^{-1}(-B) < \pi, \quad (1.5-29)$$

and λ, ϕ are defined earlier in Eq. (1.5-20).

The integration of Eq. (1.5-27) with the expression for $p(\theta_1, \theta_2)$ substituted into the integrand cannot be carried out exactly, but integration by parts yields a fairly simple series expansion:

$$R_\theta(s, \tau) = \pi^2 [1 + \Gamma(\lambda, \phi) + 2\Gamma^2(\lambda, \phi) - \frac{1}{4}\Omega(\lambda)], \quad (1.5-30)$$

where

$$\Gamma(\lambda, \phi) = \frac{1}{2\pi} \sin^{-1}(\lambda \cos \phi), \quad (1.5-31)$$

$$\Omega(\lambda) = \frac{6}{\pi^2} \sum_{n=1}^{\infty} \frac{\lambda^{2n}}{n^2}, \quad \Omega(1) = 1.$$

The phases θ_1 and θ_2 are random variables uniformly distributed from zero to 2π , that is, $p(\theta) = 1/2\pi$. Thus $\langle \theta_1 \rangle = \langle \theta_2 \rangle = \pi$, $\langle \theta_1^2 \rangle = \langle \theta_2^2 \rangle = 4\pi^2/3$. The correlation coefficient of the phases is then

$$\begin{aligned} \rho_\theta(s, \tau) &= \frac{R_\theta(s, \tau) - \langle \theta_1 \rangle \langle \theta_2 \rangle}{\sqrt{[\langle \theta_1^2 \rangle - \langle \theta_1 \rangle^2][\langle \theta_2^2 \rangle - \langle \theta_2 \rangle^2]}} \\ &= \frac{3}{\pi^2} [R_\theta(s, \tau) - \pi^2]. \end{aligned} \quad (1.5-32)$$

Substituting Eq. (1.5-30),

$$\rho_\theta(s, \tau) = 3\Gamma(\lambda, \phi)[1 + 2\Gamma(\lambda, \phi)] - \frac{1}{4}\Omega(\lambda). \quad (1.5-33)$$

The dependence of this correlation coefficient on $s\sigma$ is shown in Figure 1.5-2, where again τ has been set equal to 0. If we choose as a measure of coherence bandwidth the frequency separation for which $\rho_\theta(s, 0) = 0.5$ (analogous to the definition for the envelope correlation) we see that this

occurs when $s\sigma = \frac{1}{2}$, corresponding to a coherence bandwidth equal to $1/4\pi\sigma$, or $\frac{1}{2}$ the value for the former case. Thus if $\sigma \sim \frac{1}{4} \mu\text{sec}$, the coherence bandwidth for the phase is about 320 KHz.

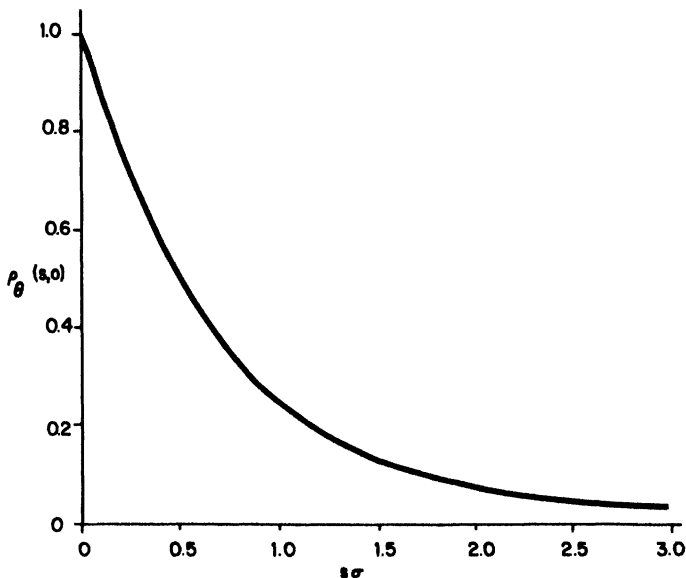


Figure 1.5-2 Dependence of the phase correlation coefficient on the frequency separation $s = \omega_2 - \omega_1$, and time delay spread σ .

1.5.4 Probability Distributions of the Phase Difference at Two Frequencies

Besides the correlation coefficient of the phases we will find the statistics of the phase difference, $\theta_2 - \theta_1$, to be of interest. Since both θ_1 and θ_2 can take any value from zero to 2π , the quantity $(\theta_2 - \theta_1)$ can have any value from -2π to $+2\pi$; thus we must be careful to avoid ambiguities of 2π in defining density functions and mean square values. First let us consider the probability density of the random variable

$$\zeta = \theta_2 - \theta_1. \tag{1.5-34}$$

From Ref. 9, p. 189, we find that

$$p(\zeta) = \int_0^{2\pi} p(\theta_1, \zeta + \theta_1) d\theta_1. \tag{1.5-35}$$

But θ_1 must satisfy two criteria:

$$\begin{aligned} 0 < \theta_1 < 2\pi, \\ 0 < \theta_1 + \zeta < 2\pi; \end{aligned} \quad (1.5-36)$$

this defines two regions for $p(\zeta)$:

$$\begin{aligned} \zeta > 0: \quad p(\zeta) &= \int_0^{2\pi-\zeta} p(\theta_1, \zeta + \theta_1) d\theta_1, \\ \zeta < 0: \quad p(\zeta) &= \int_{-\zeta}^{2\pi} p(\theta_1, \zeta + \theta_1) d\theta_1. \end{aligned} \quad (1.5-37)$$

From Eq. (1.5-28),

$$\begin{aligned} p(\theta_1, \zeta + \theta_1) &= \frac{1-\lambda^2}{4\pi^2} \\ &\times \frac{\sqrt{1-\lambda^2 \cos^2(\zeta-\phi)} + \lambda \cos(\zeta-\phi) \cos^{-1}[-\lambda \cos(\zeta-\phi)]}{[1-\lambda^2 \cos^2(\zeta-\phi)]^{3/2}}. \end{aligned} \quad (1.5-38)$$

For brevity it will be convenient in the following development to define a function F represented by Eq. (1.5-38):

$$p(\theta_1, \zeta + \theta_1) \stackrel{\Delta}{=} F[\cos(\zeta - \phi)]. \quad (1.5-39)$$

Thus $p(\theta_1, \zeta + \theta_1)$ is independent of θ_1 , so that Eq. (1.5-37) may be immediately evaluated:

$$p(\zeta) = (2\pi + |\zeta|)F[\cos(\zeta - \phi)]. \quad (1.5-40)$$

As noted earlier, $-2\pi < \zeta < 2\pi$. It will be useful to define a new variable which is confined to the region from $-\pi$ to $+\pi$, and therefore corresponds to a physically measurable, unambiguous quantity. Let

$$\xi = \begin{cases} \zeta - 2\pi, & \pi < \zeta < 2\pi \\ \zeta, & -\pi < \zeta < \pi \\ \zeta + 2\pi, & -2\pi < \zeta < -\pi \end{cases} \quad (1.5-41)$$

Then it can be shown⁹ that under this transformation of variables,

$$p(\xi) = 2\pi F[\cos(\xi - \phi)], \quad -\pi < \xi < \pi. \quad (1.5-42)$$

We now consider an experiment designed to measure the statistics of the measurable phase difference. Assume two CW signals at frequencies ω_1 and ω_2 are transmitted from the base station to two separate antennas on the mobile unit; these antennas being spaced far enough apart so that all the statistics of the signals received on the two are independent. As shown in Figure 1.5-3, the signals at frequencies ω_1 and ω_2 from each antenna are multiplied together and the difference frequency components selected by the low-pass filters. These signals are at the same frequency, namely $\omega_2 - \omega_1$, and thus a phase detector can be used to measure the phase difference, $(\theta_{2b} - \theta_{1b} - \theta_{2a} + \theta_{1a})$. Let ξ_a correspond to the measurable phase difference $\theta_{2a} - \theta_{1a}$, ξ_b to $\theta_{2b} - \theta_{1b}$, and consider the statistics of $\xi_b - \xi_a$. First let

$$w = \xi_b - \xi_a, \quad -2\pi < w < 2\pi. \quad (1.5-43)$$

The probability density $p(w)$ is then found in the same way as $p(\zeta)$, Eq. (1.5-35):

$$p(w) = \int_{-\pi}^{\pi} p(\xi_a, \xi_a + w) d\xi_a. \quad (1.5-44)$$

Under the assumption that ξ_a and ξ_b are independent (since antennas a and b are well separated), $p(\xi_a, \xi_b) = p(\xi_a)p(\xi_b)$; thus

$$p(w) = \begin{cases} \int_{-\pi}^{\pi-w} p(\xi_a)p(\xi_a + w) d\xi_a, & w > 0 \\ \int_{-\pi-w}^{-\pi} p(\xi_a)p(\xi_a + w) d\xi_a, & w < 0 \end{cases}. \quad (1.5-45)$$

We now define a new variable ψ such that $-\pi < \psi < \pi$ to correspond to measurable phase angles:

$$\psi = \begin{cases} w - 2\pi & \pi < w < 2\pi \\ w, & -\pi < w < \pi \\ w + 2\pi, & -2\pi < w < -\pi \end{cases} \quad (1.5-46)$$

Under this transformation of variables the probability density of ψ becomes

$$p(\psi) = \int_{-\pi}^{\pi} p(\xi_a)p(\xi_a + \psi) d\xi_a. \quad (1.5-47)$$

Substituting $p(\xi)$ from Eq. (1.5-42)

$$\begin{aligned}
 p(\psi) &= 4\pi^2 \int_{-\pi}^{\pi} F[\cos(\xi_a - \phi)] F[\cos(\xi_a - \phi + \psi)] d\xi_a \\
 &= 4\pi^2 \int_{-\pi}^{\pi} F[\cos y] F[\cos(y + \psi)] dy \\
 &= 4\pi^2 \int_0^{\pi} F[\cos y] \{ F[\cos(y + \psi)] + F[\cos(y - \psi)] \} dy, \quad (1.5-48)
 \end{aligned}$$

where we have made the variable change $y = \xi_a - \phi$. Inspection of Eq. (1.5-48) shows that $p(\psi)$ is independent of ϕ and symmetric in ψ , $p(-\psi) = p(\psi)$. The angle ψ thus corresponds to the magnitude of the phase difference $|(\theta_{2b} - \theta_{1b}) - (\theta_{2a} - \theta_{1a})|$ that would be measured by a phase detector in the range $-\pi$ to $+\pi$. The statistics of ψ , such as the density function $p(\psi)$ and the variance $\langle \psi^2 \rangle$ will agree with those one would measure by the experiment shown in Figure 1.5-3.

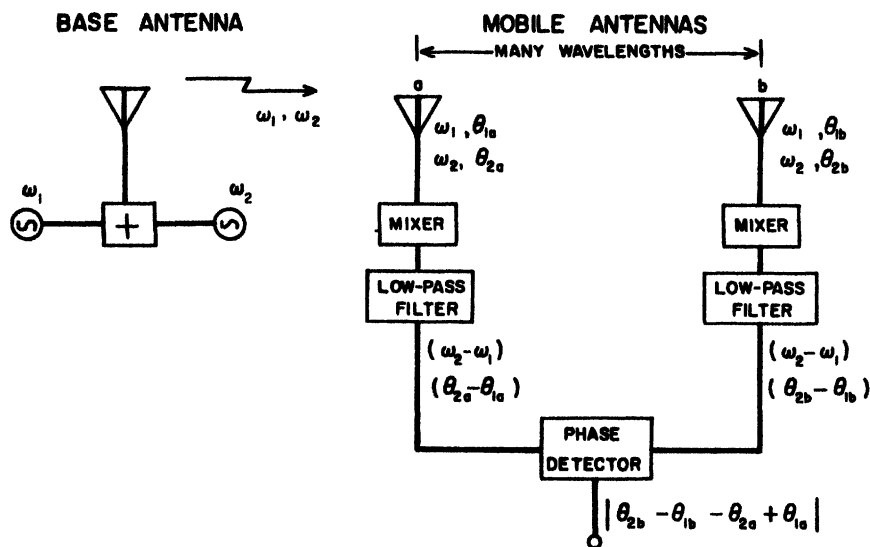


Figure 1.5-3 Experiment to measure the statistics of the phase difference between two signals at different frequencies.

The expression for $p(\psi)$ given by Eq. (1.5-48) cannot be integrated in closed form; numerical integration yields the curves of Figure 1.5-4 for

various values of the parameter λ .* As λ increases, corresponding to a decrease in σ , the phase difference tends to concentrate more about $\psi = 0$, as one would expect. Measurements¹⁷ of the density show rough agreement with Figure 1.5-4, depending on the choice of σ .

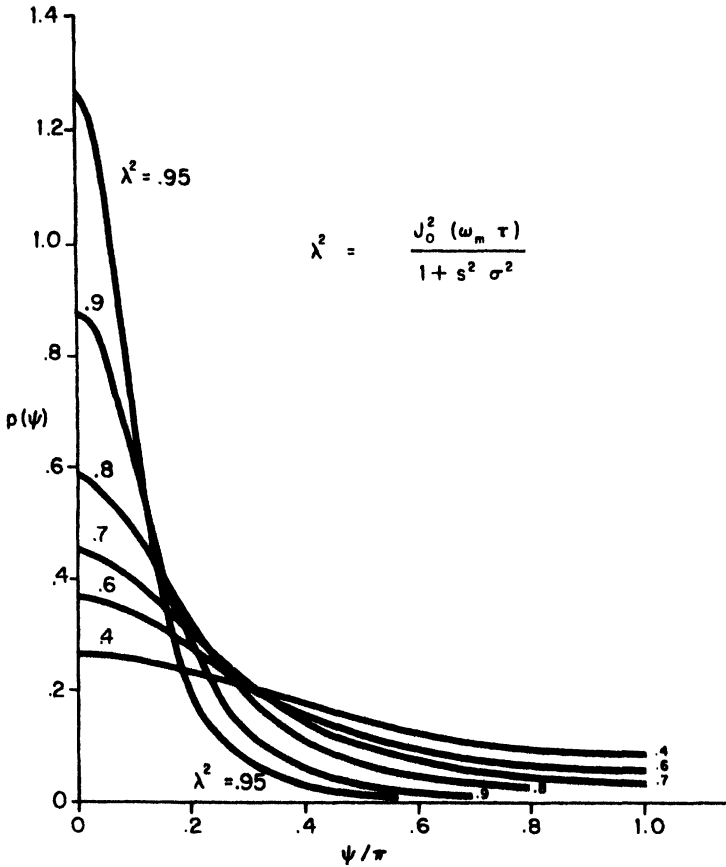


Figure 1.5-4 The probability density $p(\psi)$ of the “measurable” phase difference between signals of two different frequencies, ω_1 and ω_2 . $s = \omega_2 - \omega_1$.

*An explicit expression can be obtained for the difference between $p(0)$ and $p(\pi)$, however:

$$p(0) - p(\pi) = \pi \lambda^2 (4 - \lambda^2) (1 - \lambda^2)^{-1/2} / 32.$$

This serves as a check on the numerical integration.

The variance of ψ may be easily found from $p(\psi)$:

$$\langle \psi^2 \rangle = \int_{-\pi}^{\pi} \psi^2 p(\psi) d\psi. \tag{1.5-49}$$

Again numerical integration must be used, with the results shown in Figure 1.5-5. If $\lambda = 0$ (signals at ω_1 and ω_2 uncorrelated), $P(\psi) = 1/2\pi$; that is, ψ is uniformly distributed from $-\pi$ to $+\pi$. In this case $\langle \psi^2 \rangle = \pi^2/3$. Some measured values of $\langle \psi^2 \rangle$ are also shown in Figure 1.5-5.

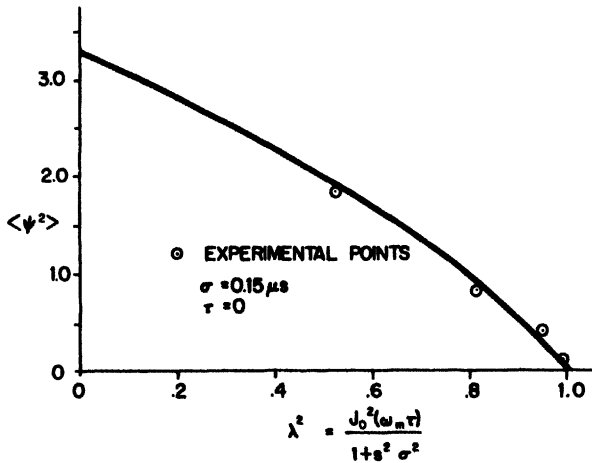


Figure 1.5-5 Mean square value of the “measurable” phase difference between signals of two different frequencies, ω_2 and ω_1 . $s = \omega_2 - \omega_1$.

1.5.5 Ratio of Signal Envelopes at Two Frequencies

As a final point of interest we will determine the probability that the signal envelope at frequency ω_2 exceeds that at ω_1 by a given amount. This would be of concern when considering interference between two signals at two frequencies transmitted from one base station. If the signals lie within the coherence bandwidth, the variation in their amplitudes due to multipath fading is appreciably correlated. A receiver that provides adequate discrimination between the desired signal (at ω_1) and the undesired signal under nonfading conditions would also do so under fading conditions in this case. However, as the frequency separation increases, the chance that

the undesired signal occasionally exceeds the desired one by a given amount will increase, with a consequent increase in interference. The probability that $r_2 > ar_1$ may be obtained from the joint density of Eq. (1.5-22):

$$\begin{aligned}
 P[r_2 > ar_1] &= \int_0^\infty dr_1 \int_{ar_1}^\infty p(r_1, r_2) dr_2 \\
 &= \frac{1}{\mu^2(1-\lambda^2)} \int_0^\infty dr_1 \int_{ar_1}^\infty r_1 r_2 \exp\left[-\frac{r_1^2 + r_2^2}{2\mu(1-\lambda^2)}\right] \\
 &\quad \times I_0\left[\frac{r_1 r_2}{\mu} \frac{\lambda}{1-\lambda^2}\right] dr_2. \tag{1.5-50}
 \end{aligned}$$

By making a change of variables $r_2 = r \cos \theta$, $r_1 = r \sin \theta$ this integral may be easily evaluated¹⁴:

$$\begin{aligned}
 P[r_2 > ar_1] &\triangleq P(a, \lambda) \\
 &= \frac{1}{2} + \frac{1}{2} \frac{(1-a^2)}{\sqrt{(1+a^2)^2 - 4\lambda^2 a^2}}. \tag{1.5-51}
 \end{aligned}$$

Equation (1.5-20) gives λ for the case of the exponential time delay distribution. Setting $\tau=0$ we can express the probability in terms of $s\sigma$, obtaining the curves of Figure 1.5-6. For $\lambda \rightarrow 0$ the curves are asymptotic to $1/(1+a^2)$, and for small values of $s\sigma$ they approach

$$P(a, s\sigma) \doteq \left[\frac{as\sigma}{1-a^2} \right]^2, \quad \text{if } a > 1. \tag{1.5-52}$$

The two earlier definitions of coherence bandwidth correspond to $s\sigma = 1$ (50% amplitude correlation) or $s\sigma = 0.5$ (50% phase correlation). These values are shown on the figure, and we can see that if the frequency separation $s = \omega_2 - \omega_1$ is less than the coherence bandwidth the probability that r_2 exceeds r_1 by an appreciable amount is very small.

1.6 SPATIAL CORRELATIONS AT THE BASE STATION

The results of preceding sections have been obtained by considering the mobile unit as a receiver. At first thought it might seem that transmitting from mobile to base should not change matters; after all, radio transmis-

sion in a linear medium obeys the reciprocity theorem! However, the reciprocity theorem must be applied with care in a scattering medium.²¹ The base station in a typical mobile radio system layout is usually located well above surrounding objects so that it has the best possible access to mobiles within its domain of coverage. The simplified model of this path places the important scattering objects (those that produce the multipath effects) within a small distance of the mobile, and more or less uniformly located around it. Up to now we have concentrated our attention on the resulting processes at the mobile; now we will examine the implications of this model with respect to the base station.

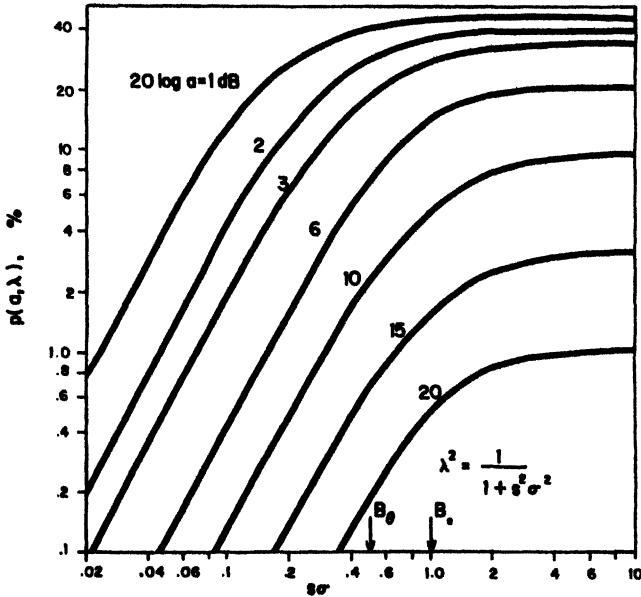


Figure 1.5-6 Probability that the signal envelope r_2 at frequency ω_2 exceeds a times that at ω_1 ; both signals transmitted from the same base station with equal power. B_0 , envelope coherence bandwidth, B_p , phase coherence bandwidth.

1.6.1 Mathematical Model

Referring to Figure 1.6-1 we assume that a ring of scattering objects whose bi-static scattering cross section is uniform are located in a circle of radius a around the transmitter at the mobile unit. The distance d from

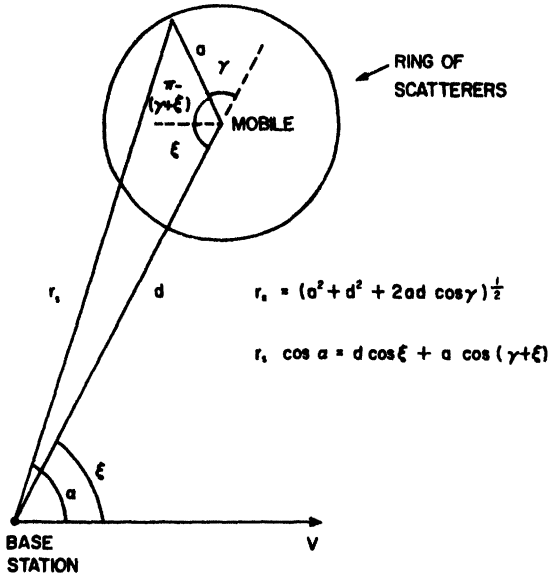


Figure 1.6-1 Scattering model for examination of spatial correlations at the base station.

mobile to the base receiver will be assumed much greater than a , so that the base does not lie within this circle. It will be convenient to start with the power spectrum approach used in Section 1.2; to this end we artificially assume that the mobile is now fixed and the base moves along the x -axis with velocity v . We need then to introduce a further assumption that d is so large that the angle ξ between v and the direction to the mobile does not change significantly during observation times of interest (i.e., the movement of the base station along the x -axis is small compared to d).

Let the distribution of power radiated from the mobile with azimuth angle γ be denoted $p(\gamma)$. The power incident on the scatterers within a circumferential length dl is then $Kp(\gamma)d\gamma$. The proportionality constant K can be set equal to unity without loss of generality. This power is scattered uniformly in angle, so that the power, $p(\alpha)$, at the base station within $d\alpha$ of the angle α is, neglecting multiplicative constant factors independent of α and γ ,

$$p(\alpha)d\alpha = p(\gamma)d\gamma. \tag{1.6-1}$$

This is also the power within df of the frequency f contained in the power spectrum $S(f)$ corresponding to the given α ; thus

$$S(f)df = p(\alpha)d\alpha = p(\gamma)d\gamma. \tag{1.6-2}$$

A complex correlation function of time τ can be defined from Eqs. (1.3-2)–(1.3-3):

$$c(\tau) \triangleq g(\tau) + ih(\tau) = \int_{f_c - f_m}^{f_c + f_m} \exp\{i[2\pi\tau(f - f_c)]\} S(f) df. \quad (1.6-3)$$

In the present case $f = f_c + f_m \cos \alpha$, but α depends on γ through the relation

$$\alpha(\gamma) = \cos^{-1} \left[\frac{\cos \xi + k \cos(\gamma + \xi)}{\sqrt{1 + 2k \cos \gamma + k^2}} \right], \quad k = \frac{a}{d} \quad (1.6-4)$$

which may easily be derived from the geometry of Figure 1.6-1. The integration on f in Eq. (1.3-21) is replaced by integration on γ , so that

$$c(\tau) = \int_{-\pi}^{\pi} e^{i\omega_m \tau \cos[\alpha(\gamma)]} p(\gamma) d\gamma. \quad (1.6-5)$$

Assuming now that the power transmitted from the mobile, b_0 , is radiated uniformly in all directions, we get

$$c(\tau) = \frac{b_0}{2\pi} \int_{-\pi}^{\pi} e^{i\omega_m \tau \cos[\alpha(\gamma)]} d\gamma. \quad (1.6-6)$$

This integral, with Eq. (1.6-4) substituted for α , cannot be explicitly evaluated. But we have assumed $a \ll d$, or $k \ll 1$, so an approximation may be obtained to various orders of k by expanding $\cos \alpha$ in powers of k :

$$\cos \alpha = \sum_{n=0}^{\infty} a_n k^n, \quad (1.6-7)$$

where the first few a_n are

$$a_0 = \cos \xi,$$

$$a_1 = -\sin \xi \sin \gamma,$$

$$a_2 = \frac{1}{2} \sqrt{1 - \frac{1}{4} \cos^2 \xi} \cos 2(\gamma - \gamma_0) - \frac{1}{4} \cos \xi, \quad (1.6-8)$$

and

$$\tan 2\gamma_0 = 2 \tan \xi. \quad (1.6-9)$$

To second order in k the integral then becomes

$$c(\tau) \doteq \frac{b_0}{2\pi} e^{i\omega_m \tau(1-k/4)^2 \cos \xi} \times \int_{-\pi}^{\pi} \exp \left\{ i\omega_m \tau \left[\frac{1}{2} k^2 \sqrt{1 - \frac{3}{4} \cos^2 \xi} \cos 2(\gamma - \gamma_0) - k \sin \xi \sin \gamma \right] \right\} d\gamma. \tag{1.6-10}$$

To carry out the integration we expand the exponential functions in terms of Bessel functions with the relation

$$e^{iz \cos x} = \sum_{n=-\infty}^{\infty} i^n J_n(z) e^{inx}. \tag{1.6-11}$$

The integral on γ can then be written

$$I = \int_{-\pi}^{\pi} \sum_{m,n=-\infty}^{\infty} (-1)^m i^n J_m(z_1) J_n(z_2) e^{i(2n+m)\gamma - 2n\gamma_0} d\gamma \\ = 2\pi \sum_{n=-\infty}^{\infty} J_{2n}(z_1) J_n(z_2) e^{in(\pi/2 - 2\gamma_0)}, \tag{1.6-12}$$

where

$$z_1 = \omega_m \tau k \sin \xi, \tag{1.6-13}$$

$$z_2 = \frac{1}{2} k^2 \omega_m \tau \sqrt{1 - \frac{3}{4} \cos^2 \xi}.$$

The envelope auto-covariance function may now be obtained from $c(\tau)$. From Eqs. (1.3-13) and (1.3-49) we see that

$$L_e(\tau) \doteq \frac{\pi}{8b_0} |c^2(\tau)| = \frac{b_0}{32\pi} II^* \\ = \frac{b_0 \pi}{8} \sum_{m,n=-\infty}^{\infty} e^{i(\pi/2 - 2\gamma_0)(n-m)} J_{2n}(z_1) J_{2m}(z_1) J_n(z_2) J_m(z_2). \tag{1.6-14}$$

The term for $m=n=0$ is a good approximation to this expansion, for third-order accuracy in k (and for fourth-order accuracy in k when $\xi=0$); thus

$$L_e(\tau) \doteq \frac{\pi b_0}{8} J_0^2(z_1) J_0^2(z_2). \tag{1.6-15}$$

1.6.2 Envelope Correlation as a Function of Antenna Separation

Since $\omega_m \tau = 2\pi v \tau / \lambda$, Eq. (1.6-15) can be regarded as a function of spatial separation $\zeta = v\tau$. We can now abandon the artificial assumption of a moving base station, and instead consider that $L_e(\zeta)$ gives the correlation between the envelopes of signals received simultaneously on two antennas at the base, separated by a distance ζ . To third order in k , Eq. (1.6-15) is directly analogous to Eq. (1.3-50) giving the auto-covariance of the E_z field seen at the mobile. Comparing arguments, we see that the base antenna separation must be a factor $(k \sin \xi)^{-1}$ times greater than that at the mobile to obtain the same correlation. Also, for $\xi = 0$ the third-order approximation gives a constant value of correlation independent of separation and equal to the value for $\zeta = 0$. Thus the fourth-order approximation is needed in this case. Estimates of the scattering circle diameter vary, but it seems obvious that it must be at least equal to the distance between buildings on opposite sides of the street where the mobile is located. This is substantiated by some experimental measurements.¹⁹ Thus $2a$ might typically be 100 ft; at a range of $d = 2$ miles, $k = 0.005$; thus the power series expansion in k appears justified.

Curves of the correlation coefficient $\rho_e \doteq J_0^2(z_1)J_0^2(z_2)$ for $k = 0.006$ are shown in Figure 1.6-2, along with some values measured at 836 MHz.²² Comparison with Figure 1.3-6 illustrates how much more rapidly the signals at the mobile become decorrelated with antenna separation. It should be emphasized that the model used here assumes *no* scatterers in the immediate vicinity of the base station; the presence of even a small number of local scatterers would have a strong effect on the correlation, particularly for $\xi = 0$.

The model also does not include the direction of motion of the mobile with respect to the line-of-sight to the base station. One would expect that motion along the line-of-sight would require greater base station antenna separation for the same correlation, compared to motion perpendicular to the line-of-sight. This effect could be included by assuming that the scatterers lie on an ellipse with major axis along the direction of motion. A refined model of this type would approach the actual disposition of the scatterers more closely.

1.7 LABORATORY SIMULATION OF MULTIPATH INTERFERENCE

The testing of mobile radio transmission techniques in the field is time-consuming and often inconclusive, due to uncertainty in the statistical signal variations actually encountered. Laboratory testing with signals that duplicate the assumed statistical properties of the signals encountered in

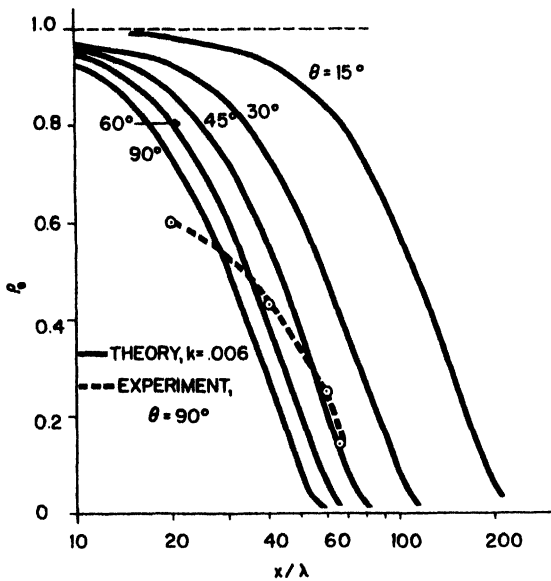
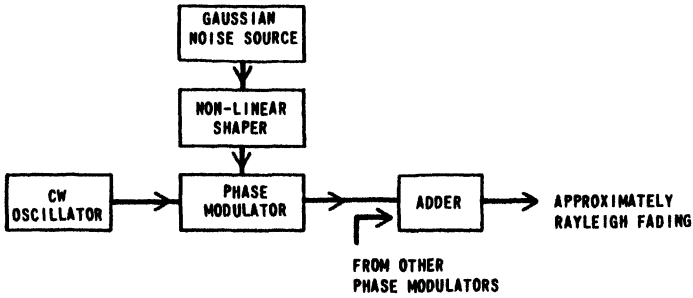


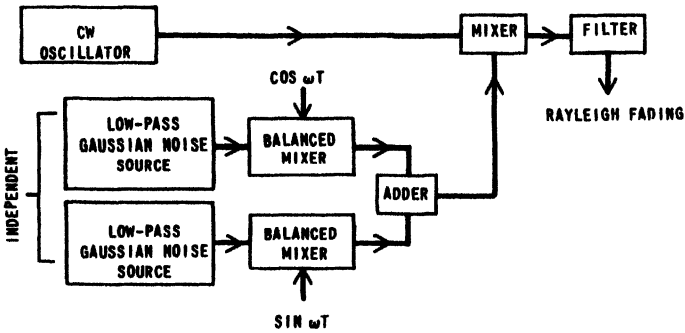
Figure 1.6-2 Correlation coefficient ρ_c between signals received on two antennas at a base station versus their separation and orientation angle θ .

the field is an attractive alternative, provided that all of the relevant properties can be simulated. Past approaches to the problem of simulating fading signals may be divided into three classes. First, tape recordings of the actual fading signals may be used.²³ In another method²⁴ a steady signal is split into several paths, each of which is then randomly phase modulated as shown in Figure 1.7-1(a). Uniformly distributed phase modulation is obtained by appropriately shaping the amplitude distribution of low-pass Gaussian noise. An approximation to Rayleigh fading is obtained by adding several such paths together. Frequency selective fading can also be produced by including path delay. However, the power spectrum of the output signal is very difficult to calculate or control. A third method²⁵ provides uniform phase modulation and Rayleigh envelope fading by amplitude modulation of the in-phase and quadrature components of a steady carrier with uncorrelated low-pass Gaussian noises, as shown in Figure 1.7-1(b). Frequency selective fading may be produced by combining several delayed fading signals. The different noise sources must have the same power spectrum to produce stationary fading, and the power spectrum of the fading signal will then be the same as the noise

spectrum. The limitation with this approach is that only rational forms of the fading spectrum can be produced, whereas the spectra encountered in mobile radio are generally nonrational, as shown by Eqs. (1.2-11)–(1.2-13). A method²⁶ to simulate mobile radio fading that produces random phase modulation, a Rayleigh fading envelope, and a time-averaged, discrete approximation to the desired power spectrum will be discussed in the remainder of this section.



(a)



(b)

Figure 1.7-1 Two types of fading simulators. (a) Simulator using uniform phase modulation. (b) Simulator using quadrature amplitude modulation.

1.7.1 Mathematical Development

We start with an expression that represents the field as a superposition of plane waves:

$$E(t) = \text{Re}[T(t)e^{i\omega_c t}], \tag{1.7-1}$$

where

$$T(t) = E_0 \sum_{n=1}^N c_n e^{i(\omega_m t \cos \alpha_n + \phi_n)}, \quad (1.7-2)$$

and

$$c_n^2 = p(\alpha_n) d\alpha = \frac{1}{2\pi} d\alpha.$$

We assume that the arrival angles are uniformly distributed with $d\alpha = 2\pi/N$; thus $c_n^2 = 1/N$, and

$$\alpha_n = \frac{2\pi n}{N}, \quad n = 1, 2, \dots, N. \quad (1.7-3)$$

We further let $N/2$ be an odd integer; then the series can be rearranged to give

$$T(t) = \frac{E_0}{\sqrt{N}} \left\{ \sum_{n=1}^{N/2-1} [e^{i(\omega_m t \cos \alpha_n + \phi_n)} + e^{-i(\omega_m t \cos \alpha_n + \phi_{-n})}] + e^{i(\omega_m t + \phi_N)} + e^{-i(\omega_m t + \phi_{-N})} \right\}. \quad (1.7-4)$$

The first term in the sum represents waves with Doppler shifts that progress from $+\omega_m \cos(2\pi/N)$ to $-\omega_m \cos(2\pi/N)$ as n runs from 1 to $N/2-1$, while the Doppler shifts in the second term go from $-\omega_m \cos(2\pi/N)$ to $+\omega_m \cos(2\pi/N)$. Thus the frequencies in these two terms overlap. The third and fourth terms represent waves with the maximum Doppler shift of $+\omega_m$ and $-\omega_m$, respectively. Without much loss of generality it will be convenient to represent the signal in terms of waves whose frequencies do not overlap:

$$T(t) = \frac{E_0}{\sqrt{N}} \left\{ \sqrt{2} \sum_{n=1}^{N_0} [e^{i(\omega_m t \cos \alpha_n + \phi_n)} + e^{-i(\omega_m t \cos \alpha_n + \phi_{-n})}] + e^{i(\omega_m t + \phi_N)} + e^{-i(\omega_m t + \phi_{-N})} \right\}, \quad N_0 = \frac{1}{2} \left(\frac{N}{2} - 1 \right) \quad (1.7-5)$$

where the factor $\sqrt{2}$ has been used so that the total power in $E(t)$ will be unchanged. The simulation should, among other things, provide a good approximation to Rayleigh fading. If N is large enough we may invoke the Central Limit Theorem to conclude that $T(t)$ is approximately a complex Gaussian process, so that $|T|$ is Rayleigh as desired. From the work of Bennett²⁷ and Slack²⁸ it follows that the Rayleigh approximation is quite

good for $N > 6$, with deviations from Rayleigh confined mostly to the extreme peaks. Further information as to the value of N may be obtained by examining the autocorrelation of $E(t)$:

$$R(\tau) = \langle E(t)E(t+\tau) \rangle = \frac{1}{2} \text{Re} [\langle T(t)T(t+\tau)e^{i\omega_c(2t+\tau)} \rangle + \langle T^*(t)T(t+\tau)e^{i\omega_c\tau} \rangle]. \quad (1.7-6)$$

The expectations are taken over the random phases ϕ_n, ϕ_m , and they occur only as sums of differences. The only terms that contribute are those involving $\phi_n - \phi_m$ with $n = m$, so that

$$R(\tau) = \frac{b_0}{N} \cos \omega_c \tau \left[4 \sum_{n=1}^{N_0} \cos \left(\omega_m \tau \cos \frac{2\pi n}{N} \right) + 2 \cos(\omega_m \tau) \right]. \quad (1.7-7)$$

We note that Eq. (1.7-7) is of the form of a carrier factor multiplied by a low-frequency factor:

$$R(\tau) = g(\tau) \cos \omega_c \tau. \quad (1.7-8)$$

We also know, from Eq. (1.3-7), that for a uniformly scattered field $g(\tau) = b_0 J_0(\omega_m \tau)$. Although this expression was derived for a continuum of arrival angles, we may suspect that if N is large enough, the quantity in brackets in Eq. (1.7-7) will closely approximate $J_0(\omega_m \tau)$. Noting that $J_0(x)$ may be defined as

$$J_0(x) = \frac{2}{\pi} \int_0^{\pi/2} \cos(x \cos \alpha) d\alpha, \quad (1.7-9)$$

the bracketed factor of Eq. (1.7-7) may be put in the form of a discrete approximation (Riemann sum) to the integral (1.7-9). We thus expect that

$$2 \sum_{n=1}^{N_0} \cos \left(\omega_m \tau \cos \frac{2\pi n}{N} \right) + \cos(\omega_m \tau) = \frac{N}{2} J_0(\omega_m \tau). \quad (1.7-10)$$

Evaluation of Eq. (1.7-10) for various values of $\omega_m \tau$ and N shows that the series gives $J_0(\omega_m \tau)$ to eight significant digits for $\omega_m \tau < 15$ with $N = 34$. The number of frequency components needed is thus $\frac{1}{2}(\frac{34}{2} - 1) = 8$. The simulation will thus produce an RF spectrum which is a discrete approximation

to the form

$$\left[1 - \left(\frac{f - f_c}{f_m} \right) \right]^{-1/2}$$

1.7.2 Realization of the Method

The simulation technique is now clear: N_0 low-frequency oscillators with frequencies equal to the Doppler shifts $\omega_m \cos(2\pi n/N)$, $n = 1, 2, \dots, N_0$, plus one with frequency ω_m are used to generate signals frequency-shifted from

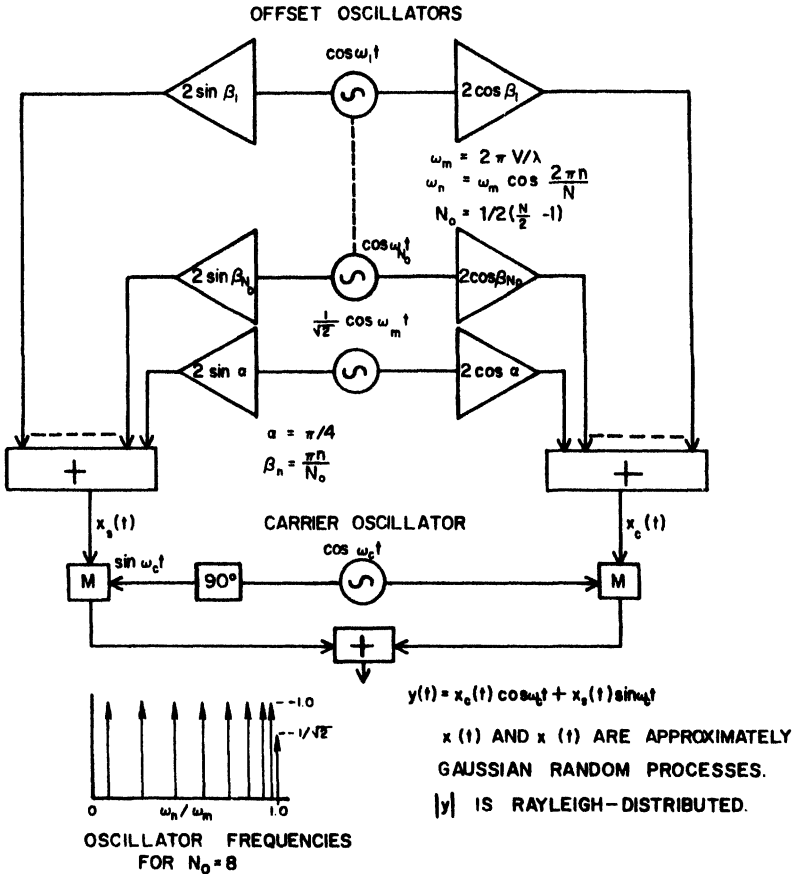


Figure 1.7-2 Simulator that duplicates mobile radio spectrum.

a carrier frequency ω_c using modulation methods. The amplitudes of all the components are made equal to unity except for the one with frequency ω_m , which is set equal to $1/\sqrt{2}$. The phases β_n are chosen appropriately so that the probability distribution of the resultant phase will be as close as possible to a uniform distribution, $1/2\pi$. A block diagram of such a simulator is shown in Figure 1.7-2 along with an illustration of the frequency spacings of the oscillators for $N_0=8$. By taking advantage of some trigonometric relationships, the proper oscillator phases are provided by amplifiers with gains set equal to $2 \cos \beta_n$ or $2 \sin \beta_n$. The outputs of the individual oscillators, with the appropriate gain factors, are first summed to produce in-phase (x_c) and quadrature (x_s) bands, which are then multiplied by in-phase and quadrature carrier components, respectively, and then summed to produce the final composite output signal $y(t)$. From the block diagram we get

$$x_c(t) = 2 \sum_{n=1}^{N_0} \cos \beta_n \cos \omega_n t + \sqrt{2} \cos \alpha \cos \omega_m t, \quad (1.7-11)$$

$$x_s(t) = 2 \sum_{n=1}^{N_0} \sin \beta_n \cos \omega_n t + \sqrt{2} \sin \alpha \cos \omega_m t. \quad (1.7-12)$$

The phase of $y(t)$ must be random and uniformly distributed from zero to 2π ; this may be accomplished in several ways, provided $\langle x_c^2 \rangle \approx \langle x_s^2 \rangle$ and $\langle x_c x_s \rangle \approx 0$. We have

$$\begin{aligned} \langle x_c^2 \rangle &= 2 \sum_{n=1}^{N_0} \cos^2 \beta_n + \cos^2 \alpha \\ &= N_0 + \cos^2 \alpha + \sum_{n=1}^{N_0} \cos 2\beta_n, \end{aligned} \quad (1.7-13)$$

$$\begin{aligned} \langle x_s^2 \rangle &= 2 \sum_{n=1}^{N_0} \sin^2 \beta_n + \sin^2 \alpha \\ &= N_0 + \sin^2 \alpha - \sum_{n=1}^{N_0} \cos 2\beta_n, \end{aligned} \quad (1.7-14)$$

$$\langle x_c x_s \rangle = 2 \sum_{n=1}^{N_0} \sin \beta_n \cos \beta_n + \sin \alpha \cos \alpha. \quad (1.7-15)$$

By choosing $\alpha = 0$, $\beta_n = \pi n / (N_0 + 1)$, we find $\langle x_c x_s \rangle \equiv 0$ and $\langle x_c^2 \rangle = N_0$, $\langle x_s^2 \rangle = N_0 + 1$. (Note that the brackets denote time averages now.) Thus $y(t)$ is a narrow-band signal centered on a carrier frequency ω_c , having Rayleigh fading characteristics, and with autocorrelation function approximately equal to $J_0(\omega_m \tau)$. Its spectrum is therefore the nonrational form given by Eq. (1.2-4), corresponding to a uniform antenna pattern, $G(\alpha) = 1$, and uniform distribution of the incident power, $p(\alpha) = 1/2\pi$. Random FM is also produced by this method. Since the carrier frequency is provided by one oscillator, it may be set to some convenient value, say 30 MHz, and voice-modulated either in amplitude or frequency for use with various reception techniques. The performance of a simulator built with nine offset oscillators ($N_0 = 8$) is illustrated in Figures 1.7-3 to 1.7-6, showing measured cumulative distribution of the envelope, autocorrelation function, RF spectrum, and random FM power spectrum. Comparison with the expected Rayleigh distribution, Bessel function autocorrelation, and theoretical RF and random FM spectra shows excellent agreement.

This technique may be extended to provide up to N_0 independently fading signals while still using the same offset oscillators. The n th oscillator is given an additional phase shift $\gamma_{nj} + \beta_{nj}$, with gains as before. By imposing the additional requirement that the output signals $y_j(t)$ be uncorrelated (or as nearly so as possible), the appropriate values for γ_{nj} and β_{nj} can be determined. The choices are not unique, but the following seems to be the simplest:

$$\beta_{nj} = \frac{\pi n}{N_0 + 1}, \quad (1.7-16)$$

$$\gamma_{nj} = \frac{2\pi(j-1)}{N_0 + 1}, \quad n = 1, 2, \dots, N_0. \quad (1.7-17)$$

By using two quadrature low-frequency oscillators per offset in place of the single oscillators shown in Figure 1.7-2, the use of phase shifters to perform the $\gamma + \beta$ shift can be eliminated. This leads to modified amplifier gains as sketched in Figure 1.7-7 for the n th offset amplifier of the j th simulator. The $N=2$ curve in the $p(R)$ graph of Figure 1.7-3 shows the resulting combined envelope statistics of a simulated two-branch maximal ratio diversity combiner (cf. Section 5.2).

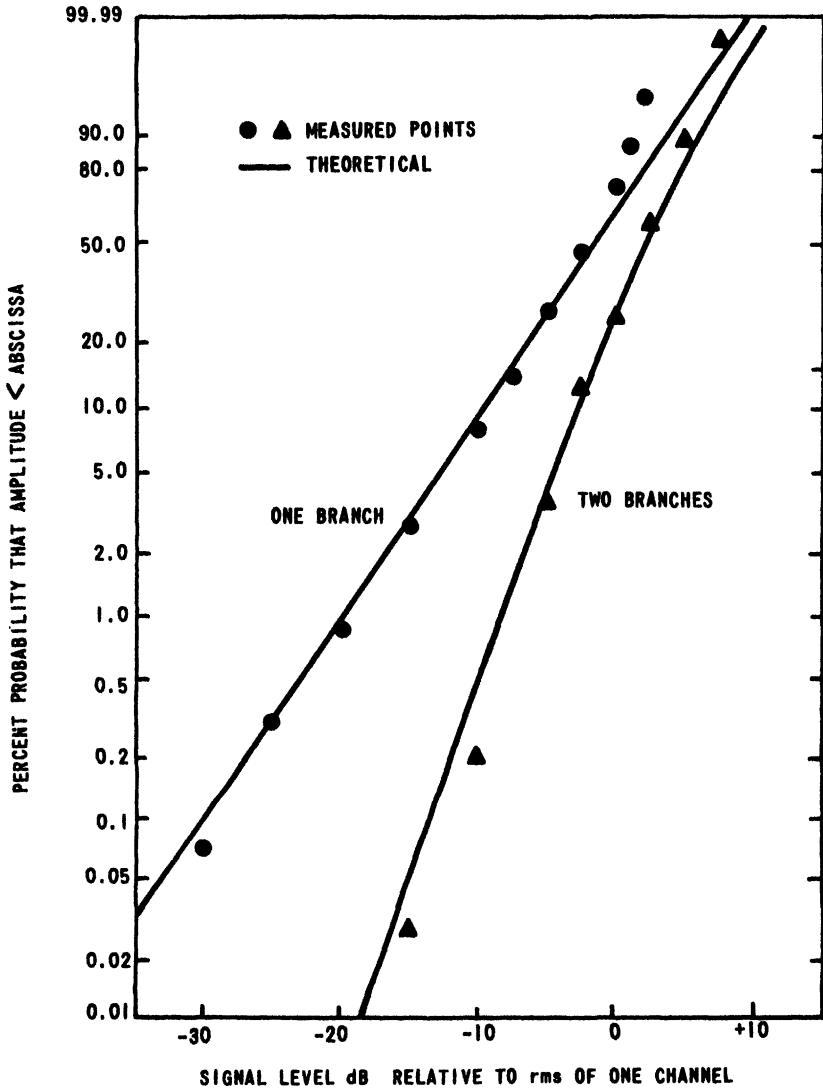


Figure 1.7-3 Probability distributions measured from the output of a fading simulator.

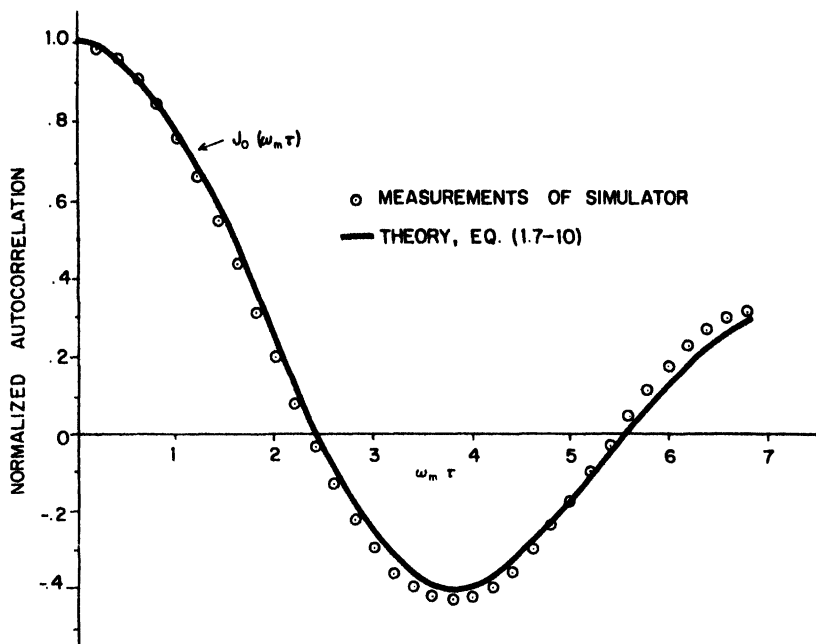


Figure 1.7-4 Comparison of theoretical autocorrelation function of the fading signal with data from a laboratory simulator.

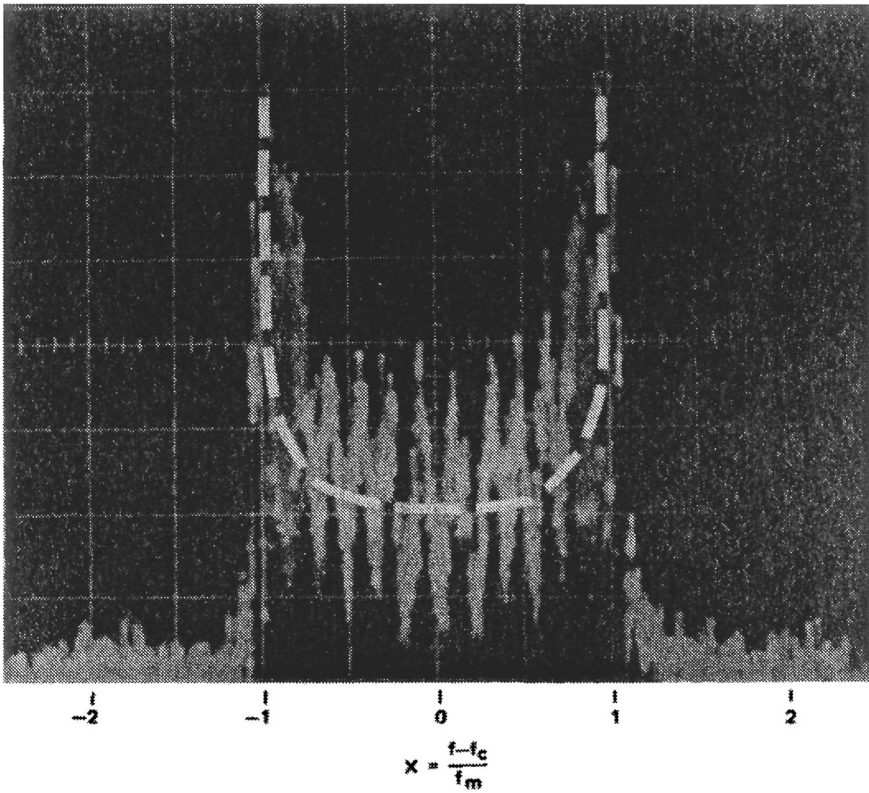


Figure 1.7-5 RF Spectrum of simulated fading carrier. Dashed line is the theoretical spectrum, $(1 - X^2)^{-1/4}$.

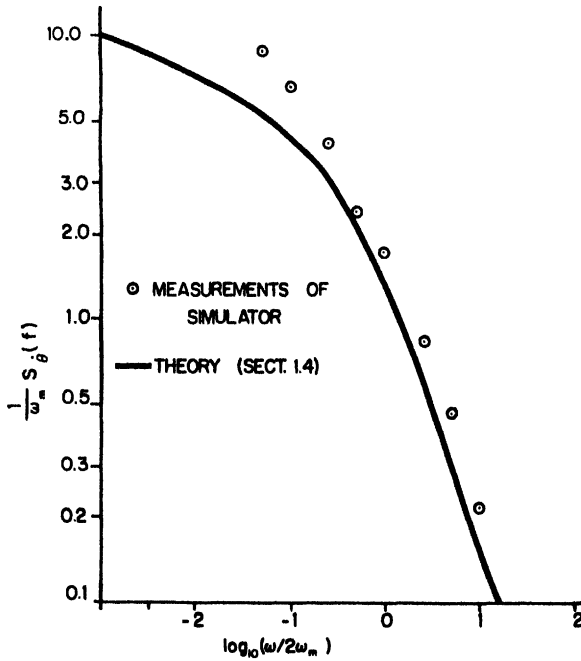


Figure 1.7-6 Comparison of theoretical spectrum of the instantaneous frequency with data from laboratory fading simulator.

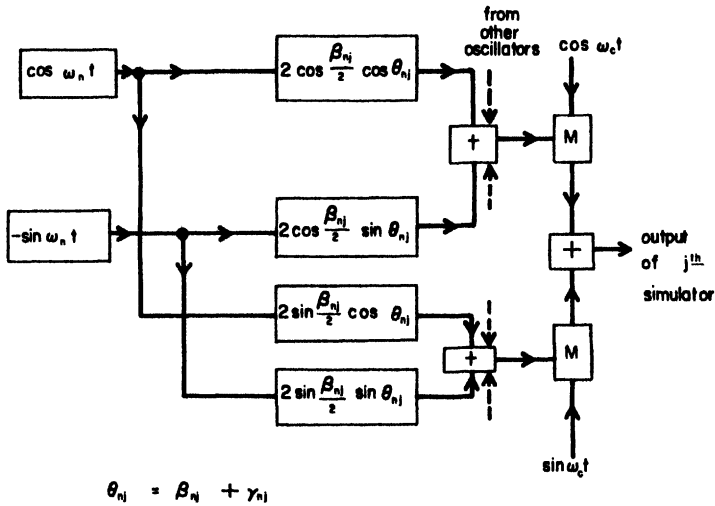


Figure 1.7-7 Use of quadrature low-frequency oscillators to provide uncorrelated fading carriers.

REFERENCES

1. W. C. Jakes, Jr. and D. O. Reudink, "Comparison of Mobile Radio Transmission at UHF and X-Bands," *IEEE Trans. Veh. Tech.* VT-16, October 1967, pp. 10-14.
2. W. R. Young, Jr., "Comparison of Mobile Radio Transmission at 150, 450, 900, and 3700 MHz," *Bell System Tech. J.* 31, November 1952, pp. 1068-1085.
3. P. M. Trifonov, V. N. Budko, and V. S. Zotov, "Structure of USW Field Strength Spatial Fluctuations in a City," *Trans. Telecomm. Radio Eng.*, 9, February 1964, pp. 26-30.
4. H. W. Nylund, "Characteristics of Small-Area Signal Fading on Mobile Circuits in the 150 MHz Band," *IEEE Trans. Veh. Tech.* VT-17, October 1968, pp. 24-30.
5. Y. Okumura, et al., "Field Strength and Its Variability in VHF and UHF Land-Mobile Radio Service," *Rev. Elect. Comm. Lab.*, 16, September 1968, pp. 825-873.
6. M. J. Gans, "A Power-Spectral Theory of Propagation in the Mobile Radio Environment," *IEEE Trans. Veh. Tech.* VT-21, February 1972, pp. 27-38.
7. R. H. Clarke, "A Statistical Theory of Mobile Radio Reception," *Bell System Tech. J.* 47, July 1968, pp. 957-1000.
8. S. O. Rice, "Mathematical Analysis of Random Noise," *Bell System Tech. J.* 23, July, 1944, pp. 282-332; 24, January 1945, pp. 46-156; "Statistical Properties of a Sine Wave Plus Random Noise," *Bell System Tech. J.* 27, January 1948, pp. 109-157.
9. A Papoulis, *Probability, Random Variables, and Stochastic Processes*, McGraw-Hill, New York, 1965.
10. P. A. Bello and B. D. Nelin, "The Effect of Frequency Selective Fading on Intermodulation Distortion and Subcarrier Phase Stability in Frequency Modulation Systems," *IEEE Trans. Comm. Sys.*, CS-12, May 1964, pp. 87-101.
11. R. S. Kennedy, *Fading Dispersive Communications Channels*, Wiley-Interscience, New York, 1969, p. 18.
12. D. C. Cox, "Doppler Spectrum Measurements at 910 MHz Over a Suburban Mobile Radio Path," *Proc. IEEE*, 59 (Tech. Corres.), June 1971, pp. 1017-1018.
13. W. B. Davenport, Jr., and W. L. Root, *An Introduction to the Theory of Random Signals and Noise*, McGraw-Hill, New York, 1958.
14. I. S. Gradshteyn and I. W. Ryzhik, *Table of Integrals, Series, and Products*, Academic, New York, 1965.
15. J. F. Ossanna, Jr., "A Model for Mobile Radio Fading Due to Building Reflections: Theoretical and Experimental Fading Waveform Power Spectra," *Bell System Tech. J.* 43, November 1964, pp. 2935-2971.
16. M. J. Gans, "A Study of the Upper Sideband Product from Mixing Gaussian Processes," to be published.

17. M. J. Gans and S. W. Halpern, "Some Measurements of Phase Coherence Versus Frequency Separation for Mobile Radio Propagation," to be published.
18. W. R. Young, Jr., and L. Y. Lacy, "Echoes in Transmission at 450 Mc from Land-to-Car Radio Units," *Proc. IRE*, **38**, March 1950, pp. 255-258.
19. D. C. Cox, "Delay-Doppler Characteristics of Multipath Propagation at 910 MHz in a Suburban Mobile Radio Environment," *IEE Trans. Ant. Prop.*, **AP-20**, September 1972, pp. 625-635.
20. E. W. Ng and M. Geller, "A Table of Integrals of the Error Functions," *J. Res. NBS-B*, **73B**, January-March 1969, pp. 1-20.
21. P. Beckmann and A. Spizzichino, *The Scattering of Electromagnetic Waves from Rough Surfaces*, The Macmillan Co., New York, 1963.
22. W. C. Y. Lee, "Antenna Spacing Requirement for a Mobile Radio Base-Station Diversity," *Bell System Tech. J.* **50**, July-August 1971, pp. 1859-1876.
23. B. Goldberg et al., "Stored Ionosphere," *IEEE First Annual Comm. Conf., Boulder, Colo.*, 1965, pp. 619-622.
24. R. C. Fitting, "Wideband Troposcatter Radio Channel Simulator," *IEEE Trans. Comm. Tech.*, **15**, August 1967, pp. 565-570.
25. R. Freudberg, "A Laboratory Simulator for Frequency Selective Fading," *IEEE First Annual Comm. Conf., Boulder, Colo.*, 1965, pp. 609-614.
26. W. L. Aranguren and R. E. Langseth, "Baseband Performance of a Pilot Diversity System with Simulated Rayleigh Fading Signals and Co-Channel Interference," *Joint IEEE Comm. Soc.-Veh. Tech. Group Special Trans. on Mobile Radio Comm.*, November 1973, pp. 1248-1257.
27. W. R. Bennett, "Distribution of the Sum of Randomly Phased Components," *Quart. Appl. Math.*, **5** January 1948, pp. 385-393.
28. M. Slack, "The Probability of Sinusoidal Oscillations Combined in Random Phase," *J. IEEE*, **93**, part III, 1946, pp. 76-86.